Orenda P.S. 13 combustion chamber (42-in. diam.): tests at atmospheric pressure

Prior, B. W.; Tyler, R. A.

Publisher's version / Version de l'éditeur:
https://doi.org/10.4224/21272069
National Research Council of Canada Aeronautical Report, 1956-01-25

SECRET

COPY NO. 5

NATIONAL AERONAUTICAL ESTABLISHMENT
CANADA

LABORATORY REPORT LR-154

ORENDA P.S. 13 COMBUSTION CHAMBER (42-IN. DIAM.): TESTS AT ATMOSPHERIC PRESSURE

BY

B. W. PRIOR AND R. A. TYLER

CLASSIFIED DOCUMENT - CONDITIONS OF RELEASE

1. THIS INFORMATION IS DISCLOSED FOR THE OFFICIAL USE, IN CANADA ONLY, OF THE RECIPIENT ORGANIZATION AND SUCH OF ITS STAFF AS MAY BE AUTHORIZED UNDER SEAL OF SECRECY.

2. THE TRANSMISSION OUTSIDE CANADA OR REVELATION OF THE INFORMATION IN ANY MANNER TO AN UNAUTHORIZED PERSON WOULD BE A BREACH OF THE SECURITY REGULATIONS OF THE GOVERNMENT OF CANADA.

OTTAWA

25 JANUARY 1956

NATIONAL AERONAUTICAL ESTABLISHMENT

Canada

LABORATORY REPORT

Gas Dynamics Section

SECRET
Laboratory Report: LR-154
Date: 25 January 1956
Lab. Order: 106-16A
File: BM49-7-18

Pages - Preface - 5
Text - 24
Appendix - 5
Figures - 32

For: Orenda Engines Limited.

Reference: Minutes of the joint meeting of A.V. Roe Canada Ltd. and N.A.E. at Ottawa, June 23, 1954.

Subject: ORENDA P.S. 13 COMBUSTION CHAMBER (42-IN. DIAM.): TESTS AT ATMOSPHERIC PRESSURE

Prepared by: B.W. Prior and R.A. Tyler

Submitted by: A.J. Bachmeier
Laboratory Head

D.C. MacPhail
Section Head

Approved by: J.H. Parkin
Director

SUMMARY

An Orenda P.S. 13 annular, vaporizing combustion chamber having a 42-in. diam. air casing has been tested at atmospheric pressure without preheat. The following matters were investigated: pressure loss, weak stability limits, weak ignition limits, outlet temperature distribution, flame pattern, combustion roughness including its causes and effects,

mechanical failures, carbon deposition, distortion due to overheating.

In most respects the performance of the combustor was satisfactory. However the cold pressure loss appeared high (27 combustor q's* at the design velocity of 109 ft./sec.) and the outlet temperature distribution appeared to require improvement.

---

* $q = \frac{\rho V^2}{2}$

where ρ = combustor inlet air density based on measured inlet total temperature and total pressure

V = combustor velocity based on maximum flow area.

TABLE OF CONTENTS

		Page
	SUMMARY	(i)
	LIST OF ILLUSTRATIONS	(iv)
1.0	INTRODUCTION	1
2.0	DESCRIPTION OF APPARATUS	2
	2.1 Test Combustion Chamber	2
	2.2 Air Supply	3
	2.3 Instrumentation	3
3.0	TESTING TECHNIQUES	5
	3.1 Total Head Pressure Loss - Cold Condition	5
	3.2 Total Head Pressure Loss - Hot Condition	6
	3.3 Weak Stability Limits	6
	3.4 Weak Ignition Limits	6
	3.5 Outlet Temperature Distribution	6
	3.6 Flame Pattern within the Combustor	7
	3.7 Analyses of Combustion Roughness	7
4.0	RESULTS AND DISCUSSION	8
	4.1 Pressure Loss	8
	4.1.1 Cold Condition	8
	4.1.2 Hot Condition	9
	4.1.3 Discussion	11
	4.2 Weak Stability Limits	11
	4.3 Weak Ignition Limits	12
	4.4 Outlet Temperature Distribution	12
	4.5 Flame Pattern within the Combustor	14
	4.6 Analysis of Combustion Roughness	15
	4.7 Mechanical Failures	17
	4.8 Carbon Deposition	18
	4.9 Distortion	18
	4.10 Summary	19
5.0	CONCLUSIONS	19
6.0	ACKNOWLEDGEMENTS	20
7.0	REFERENCE	20
	TABLES I - IV	21-25
	APPENDIX A: Calculation of Mean Total Head Pressure in Plane D	

LIST OF ILLUSTRATIONS

	Figure
Diagrammatic longitudinal section through P.S. 13 annular vaporizing combustor	1
Flame tube of P.S. 13 annular vaporizing combustor	2
P.S. 13 annular vaporizing combustor - atmospheric pressure test rig with instrumentation installed	3
Block diagram of combustion roughness analysing equipment	4
Total head pressure distributions, Quadrants No. 1, 2, 3, 4	5a-d
Total pressure loss between planes B and D and between planes D and O as a percentage of the inlet pressure in each case:	
screen in place	6
screen removed	7
Total pressure loss between planes B and D and between planes D and O in terms of combustor nominal q:	
screen in place	8
screen removed	9
Weak stability limits:	
screen in place	10
screen removed	11
Weak ignition limits:	
screen in place	12,13
screen removed	14,15
Outlet temperature distributions	16-20

LIST OF ILLUSTRATIONS (CONT'D)

	Figure
Ideal outlet temperature profile	21
Panoramic wave analyser traces from accelerometer attached to flame tube	22
Panoramic wave analyser traces from microphone	23
Panoramic wave analyser traces from transducer in fuel line	24
Analysis of combustor flame tube wall transverse vibrations	25
Analysis of combustor noise	26
Cracks in weld on inner wall of snout	27a
Cracks in weld on outer wall of snout	27b
Carbon deposition on base plate, vaporizer tubes, etc.	28,29
Semi-quantitative summary of results of tests on stability limits, ignition limits, flame patterns, outlet temperature distributions, and combustion roughness	30
Pressure readings from hole No. 1 of total head rake in Quadrants No. 1 and 3, plane D, when rake withdrawn in steps of 1/8 in.	A-1
Example of total and static pressure profiles, plane D	A-2

ORENDA P.S. 13 COMBUSTION CHAMBER (42-IN. DIAM.): TESTS AT ATMOSPHERIC PRESSURE

1.0 INTRODUCTION

An Orenda P.S. 13 annular, vaporizing combustion chamber having a 42-in. diam. air casing has been tested at atmospheric pressure by the N.A.E. at the request of Orenda Engines Limited. The flame tube was built to aircraft standards, whereas the fuel system, air casing, and other ancillary equipment (with the exception of the ignition system) were especially constructed for rig testing. The air casing is suitable for testing at both atmospheric and sub-atmospheric pressures which are available with the N.A.E. facilities. The internal geometry is, however, identical with that which would be employed in a combustor to be installed in the engine, so that the aerodynamic and combustion aspects of the test results could be applied to such a combustor.

The complete base plate of the flame tube, including stiffening ridges, was stamped out of relatively light sheet metal. This was an innovation and some interest attached to its mechanical performance.

The primary fuel manifold was supported within the snout of the flame tube and the seven primary jets were screwed into fittings in the manifold, terminating at holes through the base plate. The main fuel manifold was external to the combustor and 32 main jets protruded through the air casing and outer wall of the snout to terminate at the upstream ends of the vaporizing tubes. Except for the numbers of primary and main fuel jets and the points at which they terminated these fuel system arrangements were not those to be installed in the engine.

The following tests were performed on the combustor:

(1) Determination of the total head pressure loss under hot and cold conditions

(2) Measurements of the weak stability and ignition limits

(3) Measurements of the outlet temperature distribution

(4) Studies of the flame patterns within the combustor

(5) Studies of combustion roughness by analyses of the noise emitted by the combustor, some of the mechanical vibration modes of the flame tube, and the pressure pulsations in the fuel supply to the combustor.

In addition to these specific tests attention was given to the following points throughout the test programme:

(1) Mechanical failures of components

(2) Carbon deposition within the flame tube

(3) Distortion of the flame tube due to local overheating

2.0 DESCRIPTION OF APPARATUS

2.1 Test Combustion Chamber

A diagrammatic longitudinal section through the combustor is shown in Figure 1, and a photograph of the flame tube is shown in Figure 2.

Each main fuel jet consists of a metering orifice followed by a plain tube, any fuel atomization being effected by the flow of air past the end of the tube. The flow numbers of the 32 main fuel jets were measured and found to vary from 1.12 to 1.29. They were installed in the combustor so as to make the fuel distribution as uniform as possible.

Each primary fuel jet terminates in a small swirl atomizer.

The 16 large vanes, A, perform the functions of supporting the flame tube structurally and of removing the swirl from the air entering the combustor. This swirl remains in the air as it leaves the tenth stage stators of the compressor so that it was necessary to install in the test combustor a row of vanes simulating these stators. The rows of vanes B and C produce a swirl simulating that of the air entering the tenth stage compressor stators.

The screen is removable and consists of two pieces of wire gauze in series, one of 16 mesh with .018-in. wire and the other of 4 mesh with .050-in. wire.

Two high energy igniter plugs were installed in the chamber to protrude approximately 1/4 in. from the flame tube wall immediately downstream of the base plate, each plug being approximately 45 degrees from the bottom of the chamber. Two of the primary jets terminated immediately upstream of the spark plugs. The spark plugs were energized by an exciter box of the type currently being used on Orenda engines (24 volts, 12 joules).

2.2 Air Supply

In order to obtain sufficient air mass flow to produce the combustor design velocity it was necessary to use the available supply (31 lb./sec. at 100 p.s.i.a.) to drive an injector drawing secondary air from the atmosphere and supply the total combined air flow to the combustor. Control of the combustor air flow was obtained by throttling the compressor inlet, thus varying the pressure upstream of the injector primary nozzle. No independent control over the combustor inlet pressure and temperature was available. The pressure was always approximately atmospheric and the temperature varied in the range 50 to 100°C.

Considerable development work was necessary to obtain a total head pressure distribution at outlet of the injector mixing pipe which was satisfactorily flat and steady, and to reduce the noise emitted by the primary nozzle. A satisfactory outlet total pressure distribution was obtained by keeping the secondary air inlet clear of obstructions, carefully centring the primary nozzle in the secondary air inlet, and by providing sufficient mixing pipe length.

The noise emitted by the primary nozzle was somewhat reduced by replacing the original conical nozzle with a converging-diverging arrangement, but the noise level still remained uncomfortably high.

2.3 Instrumentation

The instrumentation planes B, D, O, and Z are indicated on Figure 1. Figure 3 is a photograph of the combustor rig showing all the rig instrumentation in place.

A description of the instrumentation installed in each of the four planes follows: (in planes B, D, and O, each of the four quadrants are identically instrumented, the quadrants being numbered clockwise from the upper right, looking downstream.)

Plane B - One static wall tapping, 1/8-in. diam., in the annulus outer wall of each quadrant.

One total head pressure rake, with seven holes at 1/2-in. increments of radius in each quadrant. The inner and outer holes are each 0.54 in. from the adjacent walls, the annulus width at plane B being 4.08 in.

Plane D - One static wall tapping, .089-in. diam., in the annulus outer wall of each quadrant.

One total head pressure rake with six holes placed at the centres of equal area annuli in each quadrant. These rakes are rotated 30 degrees from the axial direction in order to have approximately zero yaw angle with respect to the air flow direction in this plane.

One stagnation thermocouple rake with six thermocouples placed at the centres of equal area annuli in each quadrant. These rakes are also rotated 30 degrees from the axial direction. (Actually the thermocouples are about .085 in. downstream from the holes of the total pressure rakes, but this distance is not significant.)

Plane O - For cold pressure loss tests:

One static wall tapping, 1/16-in. diam., in the outer wall of each quadrant.

One averaging total head rake with three holes, 0.9 in. apart in each quadrant. The centre hole was placed at the centre of the annulus.

For hot running:

One radially traversing stagnation thermocouple, remotely operated, installed in one quadrant at a time.

Plane Z - One stagnation thermocouple 2 in. from the outer wall at top and at bottom of the duct.

Further instrumentation for the noise and vibration analyses:

An accelerometer was used to pick up mechanical vibrations of the flame tube. The accelerometer attachment (shown in Fig. 1) is a tube passing through a hole in the air

casing and welded to the flame tube. The accelerometer was mounted so that only vertical movement of the tube was detected and thus only transverse vibrations of the flame tube wall. A pressure transducer was used to pick up pressure oscillations in the main fuel line. It was installed at two positions, one in the fuel line just ahead of the manifold and the other just after the pumps. A muffled microphone was used to pick up combustor noise. The microphone was positioned about 8 ft. from the axis of the combustor, 3 ft. above the ground, and in the plane of the main fuel injectors.

The signals from the accelerometer, transducer and microphone were analysed by a panoramic wave analyser and photographs of the traces on the analyser screen were taken with a 35-mm. camera. A block diagram of the equipment layout is shown in Figure 4.

Fuel flow:

The main and primary fuel flows were measured with a combination of an orifice plate and a rotameter.

3.0 TESTING TECHNIQUES

3.1 Total Head Pressure Loss - Cold Condition

The total head pressure loss of the combustor without combustion taking place was measured over a range of air mass flows with and without the screen in place ahead of the combustor. The screen was removed in order to increase the attainable maximum combustor velocity, but this necessitated checking the effect on the inlet pressure distribution, pressure loss, and stability and ignition limits.

As mentioned above, the mass flow was controlled by throttling the compressor inlet only. Calculation of the air mass flow was based on the pressure measurements in plane B and the total temperature measurements in plane D.

The loss of total pressure was obtained from the measurement of total pressure in planes B, D, and O.

The total head pressure rakes in planes B and O were rotated in order to find the position where the readings were a maximum. This was found to occur when the holes faced virtually straight upstream. Consequently, the probes were used in this position at all times.

A nominal combustor velocity was obtained based on the air mass flow, the total pressure and temperature in plane D, and the full air casing internal cross-sectional area.

3.2 Total Head Pressure Loss - Hot Condition

No specific tests were performed to measure directly the total head pressure loss with combustion taking place because the total head pressure probes in plane O could not be used under these conditions. However, this loss was calculated from information obtained in other tests under hot and cold conditions.

3.3 Weak Stability Limits

The weak stability limits of the combustor were measured over a range of combustor nominal velocities with and without the screen. An approximation of a chosen velocity, with combustion occurring, could be obtained by adjustment of the mass flow, and then measured accurately. The fuel flow was then reduced until an observer looking upstream into the combustor outlet signalled that the first vaporizer tube (invariably one at the top of the combustor) had blown out, whereupon the fuel flow was read. The fuel flow was further reduced until the last vaporizer tube had blown out and the fuel flow read again. During reduction of the fuel flow the air mass flow remained very steady.

3.4 Weak Ignition Limits

The maximum velocity at which ignition of the chamber could be effected was determined for main fuel flows of 500, 1000, and 1500 lb./hr., and primary fuel pressures (at the manifold) of 0, 30, 50, and 100 p.s.i.g. with and without the screen.

The procedure was to switch on the ignition system, the primary fuel, and the main fuel at 3-sec. intervals and to wait a maximum of 15 sec. for ignition of the fuel to occur. If ignition occurred the test was repeated and three consecutive ignitions were necessary to constitute a "light point". The velocity was then raised in steps of approximately 5 ft./sec. and measured at each condition, until a condition was reached where three consecutive ignitions could not be obtained, this constituting a "no-light point".

3.5 Outlet Temperature Distribution

The outlet temperature distribution was measured

with the traversing stagnation thermocouple at velocities of approximately 70, 80, 90, 100 and 110 ft./sec. and fuel/air ratios of approximately .004, .008, .012, .016, and .020, the screen being in place in all cases. Since only one traversing gear was available it was necessary to install it in one quadrant at a time so that each test, consisting of a combination of one pair of the above conditions, had to be repeated four times. Each repeat test consisted of one traverse radially inwards and one outwards, measurement of velocity, and measurement of fuel flow.

3.6 Flame Pattern within the Combustor

Concurrently with the measurement of outlet temperature distribution, observations of the appearance of the flame within the combustor were made by an observer looking into the outlet from downstream. These observations were recorded as brief descriptions of the disposition of blue and yellow flame.

3.7 Analyses of Combustion Roughness

For all tests concerned with the analysis of the noise and the flame tube vibrations the combustor was operated at the maximum velocity obtainable (approximately 110 ft./sec.) with the screen in place. Fuel/air ratios of 0, .004, .008, .012, .016, and .020 were employed.

The following procedure was followed for tests at each of the above conditions. The analyser was first calibrated using the audio oscillator. The signal from the microphone was then applied to the analyser and a photograph of the analyser screen taken. This was repeated once. The signal from the accelerometer was then applied to the analyser and a photograph of the screen taken. This also was repeated once.

The analysis of pressure oscillations in the fuel line was made with the transducer in two locations as mentioned above, one close to the combustor, the other close to the pumps. With the transducer close to the pumps it was possible to pump fuel around the loop circuits using either of the two pumps available in such a way that all fuel passed through the section of line containing the transducer but none flowed to the combustor. With the transducer close to the combustor all fuel flowing through the main fuel jets passed through the line containing the transducer.

Three tests were done. In each case the analyser was calibrated first, then the signal from the transducer was applied to the analyser and a photograph was taken of the screen. In the first test the transducer was close to the combustor which was operating using pump No. 1 at a condition where combustion hum (to be discussed later) was occurring and the main fuel pressure was 100 p.s.i., the maximum allowed by the transducer operating limits. In the second test the transducer was close to the pumps, the combustor was not operating, but pump No. 1 was running. The third test was the same as the second except that pump No. 2 was running.

The analyser screen displays panoramically the Fourier analysis of the signal into frequencies between 0 and 1000 cycles/sec. The oscilloscope takes 3 sec. to make one sweep during which the analysis is displayed. Each photograph was exposed for 30 sec. so that ten sweeps were superimposed on each. This procedure showed up the presence of strongly dominant frequencies very clearly and eliminated errors which might have been caused by spurious frequencies occurring on one sweep only.

4.0 RESULTS AND DISCUSSION

4.1 Pressure Loss

4.1.1 Cold Condition

The total pressure measurements in plane B with and without the screen are plotted in Figure 5. Six only of the 11 mass flow conditions measured without the screen are plotted.

Since in all cases the total pressure profile is quite flat the mean pressure in plane B has been taken as the arithmetic average of the 28 readings from the four rakes. The mean static pressure for the plane was taken as the average of the four readings from the wall taps in each case.

It will be noted that after the screen was removed the total pressure in quadrant No. 3 was invariably lower than in the other three quadrants. To check whether this was due to the probe it was interchanged with the one in quadrant No. 1 and a test repeated. The probe in quadrant No. 3 continued to give low total pressure readings from which it was concluded that the velocity in the vicinity of the quadrant No. 3 probe was low. Although this low velocity region may

have been small, so that the readings should have been given less weight in the averaging than the others, there was no evidence to indicate this and it was decided to give all readings equal weight.

Since these measurements were performed it has been found that the swirl angle in plane D varies considerably across the annulus from the value of 30 degrees at which the plane D probes were set. The effect of varying swirl on the total pressure readings is serious but the effect on the stagnation temperature is small, and in fact the thermocouple readings varied only slightly in both radial and circumferential directions. Consequently the mean stagnation temperature in plane D was taken as the arithmetic average of the 24 thermocouple readings (see Table II).

The readings from the total head pressure rakes in plane D are tabulated in Table I. These were not plotted because, unlike plane B, individual readings were not values of total pressure at that point. The method of calculating a representative mean total head pressure in plane D from the readings obtained is described in Appendix A.

The mean total and static pressures in plane O were taken as the averages of the values in the four quadrants at each condition.

Table II summarizes the measurements in planes B, D, and O and the calculations of mass flow, combustor nominal velocity, and combustor nominal q where $q = \frac{\rho V^2}{2}$,

ρ = total density at plane D based on measured total pressure and temperature

V = combustor nominal velocity

Pressure losses between planes B and D and planes D and O in terms of percentage of inlet total pressure in each case and in terms of q are plotted in Figures 6, 7, 8 and 9.

4.1.2 Hot Condition

The results of the cold pressure loss tests and the outlet temperature distribution tests were used to calculate the increase in pressure loss due to combustion.

The total pressure at plane O was obtained from the total pressure at plane Z (calculated using the measured air mass flow and averaged exit temperature) and an estimated pressure loss in the exit diffuser between planes O and Z based on the cold loss in this section corrected for the increased temperature. This loss in terms of combustor q is small (approx. 1/2 q) and errors in its estimation have little effect on the overall hot pressure loss.

The total pressure at plane D was not measured during the outlet temperature distribution tests. Thus, to obtain its value it was necessary to calculate the loss between planes B and D. This was done by assuming that for a given plane B velocity, the loss in terms of q in plane B was independent of fuel/air ratio, and was therefore equal to that measured in the cold condition.

From the total pressure at plane D the combustor nominal velocity and q were obtained. For a given combustor velocity the incremental pressure loss due to combustion in terms of combustor q was assumed to depend on the temperature rise according to the relation:

$$\frac{\Delta P_{comb.}}{q} = \left(\frac{\text{hot loss}}{q} - \frac{\text{cold loss}}{q}\right) = K\left(\frac{T_o}{T_D} - 1\right)$$

where K = a constant

T_o = combustor outlet temperature (plane O)

T_D = combustor inlet temperature (plane D)

A summary of the hot pressure loss calculations is given in Table III from which the mean value for K of 4.36 is obtained.

The symbols used to designate the tests have the following meanings:

	A	B	C	D	E
Nominal velocity, ft./sec.	70	80	90	100	110
	1	2	3	4	5
Nominal fuel/air ratio	.004	.008	.012	.016	.020

The tests tabulated in Table III are those in which the outlet temperature distribution was measured in all four quadrants. At other combinations of velocity and fuel/air ratio the distribution was measured in one or more quadrants but the results were not considered useful and have not been included.

4.1.3 Discussion

The cold pressure loss at the design velocity of 109 ft./sec. is 14.5 percent or 27.0 q (averaged from the values with and without the screen). The results of the cold and hot pressure loss tests can be extrapolated to the engine maximum condition where the combustor inlet temperature is about 570°K. and the outlet temperature is 1300°K. to give a pressure loss of 11 percent or 32 q.

The non-dimensional pressure loss (32) is relatively high by normal standards (25 - 30), particularly in view of the high design velocity employed in this combustor, the combination of factors resulting in a high percentage pressure loss on the engine (11 percent cf. about 5 percent normal), leading to a gross thrust penalty of roughly 5 percent.

The effect of the screen on the total pressure distributions in planes B and D is small though not negligible. It is considered reasonable however to employ the same averaging methods both with and without the screen to obtain the mean total pressure in planes B and D.

4.2 Weak Stability Limits

The results of the weak stability limit tests are plotted in terms of air/fuel ratio against velocity with the screen in place in Figure 10 and with the screen removed in Figure 11. (It should be pointed out that a vaporizer tube near the top of the combustor is invariably extinguished first because of the relatively lower fuel static head which causes a lower fuel flow.)

Removal of the screen had virtually no effect on the air/fuel ratio at which the first vaporizer tube was extinguished for velocities of 95 ft./sec. and greater. However, the air/fuel ratio at which the last vaporizer tube was extinguished in the same velocity range appears to have been definitely lowered. This may be a real effect of change in the inlet air distribution since the last tube to be extinguished burns with a very feeble flame, or it may simply represent scatter in the results.

The weak stability limit air/fuel ratio is about what one would expect for a vaporizing combustor. For instance, in Reference 1 where a very similar combustor test was described, the limit at a velocity of 80 ft./sec. was 400 when the inlet pressure was 26 in. Hg abs. Extrapolating the results of Reference 1 and the present results to the same pressure and velocity conditions would result in about the same weak stability limit air/fuel ratio.

4.3 Weak Ignition Limits

The results of the weak ignition limit tests with the screen in place are plotted in Figure 12 in terms of velocity against primary fuel pressure for different main fuel flows, and are cross-plotted in Figure 13 in terms of velocity against main fuel flow for different primary fuel pressures. The results with the screen removed are plotted in the same terms in Figures 14 and 15.

Removal of the screen seems to have reduced the limiting ignition velocity at most combinations of main and primary fuel flows. However in at least one case (namely no primary fuel and 1000 lb./hr. main fuel) the limit has been raised by 5 ft./sec. It is thus impossible to draw any conclusion. In fact the primary fuel and ignition arrangements are in too tentative a state to allow any worthwhile comparison with other systems or conclusions as to their effectiveness.

From Figure 30 it can be seen that the ignition limit curves at primary fuel pressures of 50 and 100 p.s.i. extend into the weak extinction regions of the combustor. Presumably, if the primary fuel were turned off after ignition had been accomplished in these regions one or more of the vaporizer tubes would be automatically extinguished, but no tests were conducted to test the correctness of this prediction.

4.4 Outlet Temperature Distribution

Since, for a given combination of nominal velocity and fuel/air ratio, four separate tests had to be made in order to obtain outlet temperature traverses in the four quadrants, the measured results from the four quadrants are not directly comparable from the point of view of determining the circumferential temperature distribution. The measured results were therefore corrected for the effects of variation in the actual fuel/air ratio and the inlet temperature, the

two quantities which would have the greatest effect on the outlet temperature. The measured outlet temperatures were corrected to a common standard inlet temperature and fuel/air ratio by a degree per degree correction based on the difference between the actual inlet temperature and the standard temperature in the first case, and on the difference between the theoretical temperature rises corresponding to the actual fuel/air ratio and the standard fuel/air ratio in the second case. The standard inlet temperature and fuel/air ratio were taken to be the arithmetic means of the actual values. Since, of course, the actual values all apply to the same nominal condition these corrections were small.

The outlet temperature distributions are plotted in Figures 16, 17, 18, 19 and 20.

The temperature spread index, I, defined as

$$I = \frac{T_{max} - T_{mean}}{T_{mean}}$$

was calculated from values of temperature as plotted. It was also calculated on the assumption of an inlet temperature of 300°C., the design value, rather than on the actual inlet temperature. The results of these calculations are shown in Table III.

A comparison of the outlet temperature profiles obtained with the ideal profile, which is shown in Figure 21, indicates that some improvement is necessary. The temperature spread index of the ideal profile is low in relation to those obtained and the peak is 1.3 in. out from the centre line, whereas the peaks of the profiles obtained are generally 0.5 in. out.

The circumferential temperature distribution is rather poor when the fuel/air ratio is .012 or greater for all velocities. In particular, the temperature near the inner wall in quadrant No. 3 is generally low, and in several cases this is coupled with a relatively high peak temperature in the same quadrant. The reason for this poor distribution in quadrant No. 3 is not known; no persistent abnormality in the flame pattern in this region was observed.

4.5 Flame Pattern within the Combustor

The results of the observations of the flame patterns within the combustor are given in Table IV.

Little information on the axial length of the flame could be obtained since the observations were made from well downstream of the outlet. In some cases however, the flame extended through the turbine annulus (plane 0) in the form of long thin tongues extending 10 to 15 in. downstream of the annulus and lasting a fraction of a second. These observations are recorded in the table.

The combustor conditions of high fuel/air ratio and low velocity which produce these long flames may occur during acceleration of the engine from low speed and indicate the desirability of measures to ensure more rapid mixing and burning of the fuel at these conditions.

At fuel/air ratios of .012 or less and at all velocities, one of the vaporizer tubes at about 8 o'clock, looking upstream, produced a bright yellow spot of flame almost invariably. In the photographs of the combustor interior, discussed later (Fig. 28 and 29), this tube can be seen to have a heavier deposit of carbon than any of the adjacent tubes.

At one point during the testing, the fuel jet supplying this tube was interchanged with one from the opposite side of the combustor. The spot of flame, however, remained in the same place, suggesting that it was caused by some abnormality of the vaporizer tube. When the combustor was dismantled after the testing was completed, this vaporizer tube was examined and the only abnormality which could be seen was a slight dent in the wall at its entrance. The dent may possibly have deflected some of the fuel from the jet to the outside of the wall of the tube rather than allowing it to pass down the inside. Fuel burning on the outside of the tube would produce the effects observed.

As mentioned in the introduction, the mechanical performance of the base plate was of interest, and it was expected that the most serious condition would exist when the combustor was burning weak with the flame close to the base plate. Although the axial position of the flame could not be determined, it will be noted from Table IV that at 90 ft./sec. and .004 fuel/air ratio the base plate at the

bottom of the combustor could be seen to be glowing red, indicating tnat the flame was very close to it. No damage to the base plate resulted from this condition.

4.6 Analysis of Combustion Roughness

A fairly high pitched hum became audible at any combustor velocity when the fuel/air ratio was about .012 and a rumble became audible at a slightly richer condition. The rumble increased somewhat in volume as the fuel/air ratio was increased up to a value of .020, the maximum used. At this point the rumble did not appear serious and did not cause any visible movement of the flame tube or rig.

These noises were attributed to combustion roughness or instability. The results of their analysis are described below.

Photographs of the screen of the panoramic analyser are shown in Figures 22, 23 and 24.

The traces obtained from the accelerometer attached to the flame tube were analysed by determining the frequencies of the most prominent peaks appearing (utilizing the calibration traces), and by measuring the height of these peaks by means of the background grid. The heights were then converted to values of root-mean-square displacement of the flame tube wall by means of the expression:

$$D = \frac{4.08\ h \times 10^{a/20}}{f^2}$$

where D = displacement, in. r.m.s.

h = height of peak, grid divisions

a = attenuator setting, decibels

f = frequency, cycles/sec.

The results are shown in Figure 25.

The traces obtained from the microphone were analysed by determining the frequency and height of the most prominent

peaks again and converting the heights to values of relative sound intensity with respect to the intensity of the 360-cycle/sec. component at a fuel/air ratio of zero by means of the expression:

$$R = 20 \log_{10} \frac{h}{h_o} + a - a_o$$

where R = relative sound intensity, decibels

h = height of peak, grid divisions

h_o = height of 360 cycle/sec. peak at F/A = 0

a = attenuator setting, decibels

a_o = attenuator setting at F/A = 0

The results are shown in Figure 26.

The audible hum which starts at a fuel/air ratio of .012 at any velocity is presumably the 360-cycle/sec. component of the noise shown in Figure 26. This component is present in the noise at all fuel/air ratios down to zero, and just why it becomes so prominent at a certain critical value is not known. At the same fuel/air ratio a flame tube vibration component of virtually the same frequency makes a sudden appearance as seen in Figure 25. This flame tube vibration component may be either the cause or an effect of the hum.

It was thought that this vibration frequency might be correlated with a fuel pressure pulsation frequency reaching the combustor, and it was for this reason that the analysis of the fuel pressure pulsations was made.

The traces obtained from the transducer had, in each case, only one significant peak. The heights of these peaks were not required but only their frequencies. The frequencies are:

Test No. 1 - 272 cycles/sec.

Test No. 2 - 285 cycles/sec.

Test No. 3 - 433 cycles/sec.

These results indicate that pressure pulsations produced by the supplying pump carry through the fuel line to the combustor, but the two frequencies arising from the two pumps differ too greatly from 360 cycles/sec. to indicate any correlation.

The remaining components of the noise and flame tube vibrations, since they are present at all fuel/air ratios including zero, are probably produced by the noise emitted by the injector. In particular, the 720-cycle/sec. component which is strong throughout probably corresponds to the high pitched screech of the injector.

It will be noted that the rumble, which appears at the higher fuel/air ratios, does not appear to result in any prominent low frequency components in the analysis. This is probably because the rumble is aperiodic and not amenable to this type of analysis.

It is believed that the onset of combustion roughness was shifted into a lower fuel/air ratio region by the low inlet temperature than would be the case if the inlet temperature were at the design value of 300°C. Also, at the design inlet temperature any combustion roughness could be expected to be milder.

4.7 Mechanical Failures

Three types of minor mechanical failure were encountered during the testing. These are described below.

The flanges joining the various parts of the outer casing and ducting of the rig were held together by "Marmon" couplings. After the major part of the testing had been completed a growing fatigue crack was noticed in one of these couplings. The coupling was replaced before it caused any trouble.

The primary fuel jets were screwed into the primary fuel manifold and held by a piece of locking wire. One of these jets became unscrewed after a fracture of the wire, and the resulting leak necessitated termination of the ignition limit tests. The cause of the leak could not be determined until the rig was dismantled at the end of the testing program, at which time it was found that another jet was loose although the wire was intact. The remaining five jets were unaffected.

When the rig was dismantled after the testing was completed, several cracks were found at the entry of the flame tube snout. These cracks were all in the regions of the welds where the sections of the straightening vanes (A, Fig. 1) were welded into the snout. Photographs of some of these cracks are shown in Figure 27. The cracks did not interfere with the functioning of the flame tube during the testing.

The mechanical failures were probably due to vibrations caused by the injector noise rather than vibrations resulting from combustion roughness. The total length of time for which the combustor was operated at conditions of rough combustion was about 13 hours, whereas the total time that air was blown through the combustor by the injector was about 100 hours. During all this time the flame tube and presumably all parts of the rig were subjected to very intense vibrations at 720 cycles/sec.

4.8 Carbon Deposition

Operation of the combustor at high fuel/air ratio produced very light carbon deposition on the base plate, primary air mixing slots, vaporizer tubes, and parts of the flame tube walls adjacent to the base plate. This deposition can be seen in Figure 28. The pictures were taken at the conclusion of a test period involving 22 to 23 hours' actual burning time over a range of fuel/air ratios from .004 to .022 and chamber velocities from 40 to 110 ft./sec. About 5 hours of this time were spent at the high temperature condition. No serious carbon build-up in any part of the combustor was observed at any time during the testing.

Operation of the combustor at low fuel/air ratio removed much of any carbon deposition which had resulted from previous rich operation. For instance, the photographs in Figure 29 were taken after a few minutes of low fuel/air ratio operation following the photographs in Figure 28. It can be seen that much of the carbon has been removed.

4.9 Distortion

No distortion of any part of the base plate, flame tube walls, or conical sections of the flame tube at the outlet was observed at the completion of the testing.

However, some slight effects of local overheating can be seen in Figure 2. The dark patches on the first

section of the flame tube wall downstream from the snout are regions which have turned blue as a result of having been raised to a high temperature.

It is to be expected that some distortion of the flame tube, particularly the conical sections at the outlet, might occur at the design temperature rise if the inlet temperature were the design value since the temperature level throughout the combustor would be raised. However, the temperature of the base plate would not be unduly high except under the fairly unusual conditions of very weak burning, and in view of its performance in these tests it would not be expected to give trouble.

4.10 Summary

A semi-quantitative summary of the results of the tests on stability limits, ignition limits, flame patterns, outlet temperature distribution, and combustion roughness is shown in Figure 30. The stability and ignition limit results have been plotted in terms of velocity vs. fuel/air ratio and are averages of the results with and without the screen.

The total operating time of the combustor can be summarized as follows:

Total operating time, hot and cold ≈ 100 hr.

Total combustion time ≈ 25 hr.

Total time at rich (rough) combustion conditions ≈ 13 hr.

5.0 CONCLUSIONS

The cold pressure loss appears to be high. The results indicate a pressure loss on the engine at maximum rating of about 11 percent of combustor entry total pressure.

The weak stability limit near atmospheric pressure appears to be satisfactory.

The outlet temperature distribution requires improvement to bring the radial distribution more in line with the ideal and to reduce circumferential variation.

Measures to ensure more rapid mixing within the chamber at rich, low velocity conditions are indicated to prevent long flames which extend through the turbine annulus.

The performance of the light sheet metal base plate was satisfactory.

Operation of the combustor at the design inlet temperature of 300°C. ought to ameliorate the combustion roughness encountered at lower inlet temperatures but may lead to some distortion of the flame tube at the design temperature rise.

6.0 ACKNOWLEDGEMENTS

The authors wish to acknowledge the assistance given by the following members and former members of the staff of the N.A.E.: Mr. J.P. Beauregard who assisted in much of the work in the early stages, Mr. F. Cheers who carried out the development of the injector, and Messrs. E. Bowler and G. Wright of the Aircraft and Allied Instrument Laboratory who supplied and operated the electronic analysing equipment.

7.0 REFERENCE

1. Pouchot, W.D.
Hamm, J.R.
Characteristics of a Vaporizing Combustor for Aviation Gas Turbines.
A.S.M.E. 53-A-182, Nov.-Dec. 1953.

/LES

TABLE Ia

READINGS FROM TOTAL HEAD PRESSURE RAKES
IN PLANE D, SCREEN IN PLACE

Quad	Hole Position on Rake					
	Inner Hole 1	2	3	4	5	Outer Hole 6
Ref. 1						
1	30.15	31.60	31.75	31.70	31.25	31.85
2	30.00	31.75	31.75	31.60	31.35	31.75
3	30.00	31.60	31.75	31.65	31.25	31.85
4	30.05	31.70	31.75	31.60	31.20	31.65
Ref. 2						
1	30.15	32.00	32.30	32.25	31.60	32.35
2	30.00	32.25	32.25	31.95	31.75	32.25
3	30.40	32.05	32.20	32.15	31.65	32.40
4	30.05	32.25	32.25	32.05	31.55	32.15
Ref. 3						
1	30.10	32.85	33.25	33.20	32.30	33.30
2	29.95	33.20	33.25	32.80	32.50	33.25
3	30.45	32.95	33.15	33.00	32.40	33.40
4	30.05	33.15	33.20	32.95	32.30	33.10
Ref. 4						
1	30.10	33.80	34.40	34.40	33.15	34.40
2	29.85	34.35	34.40	33.70	33.45	34.40
3	30.40	34.00	34.30	34.15	33.30	34.55
4	29.95	34.30	34.35	33.90	33.15	34.20
Ref. 5						
1	29.90	34.80	35.85	35.85	34.25	35.35
2	29.55	35.70	35.25	34.80	34.45	35.75
3	30.25	35.15	35.70	35.40	34.25	35.70
4	29.65	35.65	35.75	35.15	34.20	35.55
Ref. 6						
1	29.85	35.25	36.60	36.60	34.85	35.60
2	29.45	36.50	36.05	35.90	34.55	-
3	30.10	35.75	36.45	36.10	34.80	36.00
4	29.60	36.35	36.50	35.80	34.75	36.30

TABLE Ib

READINGS FROM TOTAL HEAD PRESSURE RAKES
IN PLANE D, SCREEN REMOVED

Quad	Hole Position on Rake						Quad	Hole Position on Rake					
	Inner Hole 1	2	3	4	5	Outer Hole 6		Inner Hole 1	2	3	4	5	Outer Hole 6
Ref. 1							Ref. 7						
1	30.05	32.15	32.50	32.30	31.65	32.40	1	29.55	35.60	37.90	37.65	35.55	36.15
2	29.80	32.40	32.45	32.05	31.85	32.35	2	28.90	37.25	37.75	36.30	35.65	36.95
3	29.70	32.65	32.65	32.25	31.80	32.45	3	29.00	37.85	38.15	36.90	35.70	37.15
4	30.05	32.45	32.70	32.35	31.80	32.50	4	29.55	36.55	38.00	37.20	35.55	36.40
Ref. 2							Ref. 8						
1	30.45	32.95	33.45	33.25	32.45	33.30	1	29.85	36.05	38.35	38.00	35.95	36.55
2	30.20	32.40	33.45	32.85	32.65	33.30	2	29.65	37.55	38.15	37.65	36.10	37.40
3	30.10	33.55	33.60	33.05	32.50	33.15	3	29.40	38.25	38.55	37.15	36.00	36.55
4	30.30	33.25	33.60	33.15	32.50	33.40	4	29.85	36.95	38.45	37.60	35.90	36.90
Ref. 3							Ref. 9						
1	29.95	33.30	34.15	33.90	32.80	33.95	1	29.50	37.15	39.90	39.50	37.20	36.20
2	29.65	34.05	34.20	33.45	33.00	33.85	2	28.80	39.30	39.60	37.70	36.65	36.70
3	29.50	34.05	34.20	33.65	32.85	33.90	3	29.10	39.85	39.95	38.30	36.75	37.50
4	30.05	33.75	34.20	33.75	32.85	33.90	4	29.65	38.30	39.85	38.95	37.05	36.00
Ref. 4							Ref. 10						
1	30.40	33.75	34.50	34.25	33.15	34.85	1	29.55	37.15	39.80	39.40	37.10	36.20
2	30.05	34.50	34.60	36.75	33.50	34.40	2	28.80	39.30	39.65	37.75	36.65	36.70
3	29.90	34.70	34.80	34.05	33.35	34.15	3	29.05	40.00	40.00	38.40	36.70	37.40
4	30.30	34.20	34.70	34.10	33.30	34.45	4	29.65	38.50	40.05	39.10	37.15	35.90
Ref. 5							Ref. 11						
1	30.30	34.75	35.85	35.60	34.15	35.45	1	29.65	37.75	40.50	39.95	37.60	36.50
2	29.85	35.70	35.45	34.90	34.55	35.60	2	29.00	40.15	40.30	38.05	37.05	36.90
3	29.70	36.10	36.30	35.30	34.40	35.25	3	29.39	40.75	40.65	38.85	37.25	37.30
4	30.15	35.25	36.15	35.40	34.30	35.65	4	29.70	39.35	40.70	39.50	37.45	36.00
Ref. 6													
1	30.15	34.80	36.25	35.90	34.30	35.60							
2	29.60	35.85	36.15	35.00	34.60	35.70							
3	29.55	36.20	36.45	35.45	34.55	35.90							
4	30.00	35.35	36.25	35.65	34.40	35.70							

SUMMARY OF RESULTS OF COLD PRESSURE LOSS MEASUREMENTS

Ref. No.	Plane B		Plane D			Plane O		Mass Flow lb./sec.	Velocity ft./sec.	q in. Hg
	Total Press in. Hg Abs.	Static Press in. Hg Abs.	Temp. °K.	Total Press in. Hg Abs.	Static Press in. Hg Abs. (Outer Wall)	Total Press in. Hg Abs.	Static Press in. Hg Abs.			
	SCREEN IN PLACE									
1	31.85	31.15	349	31.63	30.12	30.07	29.63	34.72	67.8	0.0674
2	32.39	31.51	354	32.09	30.17	30.11	29.53	39.17	76.45	0.0857
3	33.40	32.20	361	32.98	30.22	30.15	29.35	45.4	87.9	0.1142
4	34.63	33.10	369	34.04	30.35	30.22	29.13	51.45	98.7	0.1454
5	36.14	34.23	372	35.24	30.45	30.28	28.86	58.25	108.8	0.1814
6	36.94	34.83	375	35.84	30.56	30.30	28.79	61.6	114.0	0.2010
	SCREEN REMOVED									
1	32.52	31.54	320	32.46	30.06	30.02	29.34	43.2	75.4	0.0933
2	33.55	32.33	331	33.16	30.43	30.36	29.56	47.9	84.6	0.1160
3	34.16	32.69	328	33.86	30.16	30.05	29.05	53.3	91.3	0.1392
4	34.71	33.13	336	34.17	30.54	30.38	29.36	54.7	95.2	0.1491
5	36.13	34.18	342	35.33	30.70	30.47	29.10	61.3	104.9	0.1840
6	36.32	34.30	343	35.50	30.52	30.30	28.89	62.6	107.0	0.1917
7	38.05	35.68	347	36.88	30.52	30.19	28.48	68.7	114.4	0.2250
8	38.51	36.06	349	37.23	30.90	30.56	28.76	70.0	116.0	0.2322
9	40.06	37.38	355	38.14	30.95	30.48	28.38	73.8	121.5	0.2567
10	40.16	37.41	350	38.13	30.90	30.43	28.35	75.4	122.5	0.2645
11	40.82	38.02	352	38.63	31.17	30.68	28.50	76.6	123.5	0.2713

TABLE III

SUMMARY OF RESULTS OF HOT PRESSURE LOSS CALCULATIONS AND OUTLET TEMPERATUE DISTRIBUTION MEASUREMENTS

Test	Air Mass Flow lb./sec.	Total Pressures in. Hg Abs.				Inlet Temp. °K.	Combustor Velocity ft./sec.	Combustor q in. Hg	Fuel / Air Ratio	Outlet Temp. °K.	K	Temperature Spread Index, Percent	
		Plane B	Plane D	Plane O	Plane Z							Based on Actual Inlet Temp.	Based on Inlet Temp. = 300°C.
A-5	33.66	32.43	32.23	30.11	30.08	354	65.4	0.063	.0227	1130	4.83	18.8	15.0
B-3	38.78	32.96	32.68	30.12	30.09	359	75.3	0.084	.0129	856	4.92	14.1	10.3
B-5	40.47	33.55	33.24	30.23	30.18	363	78.1	0.090	.0209	1075	4.74	17.3	13.7
C-1	45.44	33.51	33.09	30.08	30.05	362	88.0	0.114	.0041	546	2.95	11.0	6.2
C-3	46.24	34.33	33.89	30.25	30.20	369	88.6	0.117	.0124	842	4.99	16.2	11.9
C-5	48.16	35.14	34.67	30.43	30.37	370	90.9	0.125	.0201	1049	4.80	19.2	15.2
D-1	52.32	34.88	34.27	30.17	30.13	368	99.4	0.149	.0041	552	3.40	10.0	5.8
D-3	52.74	35.84	35.21	30.40	30.34	374	99.0	0.149	.0123	846	5.07	16.2	12.0
D-4	54.29	36.32	35.64	30.54	30.47	376	101.3	0.158	.0160	967	3.94	16.7	13.0
E-2	59.18	37.04	36.10	30.45	30.39	379	109.8	0.186	.0082	714	3.85	12.7	8.8
E-3	58.54	37.29	36.42	30.57	30.50	379	107.7	0.180	.0122	857	4.44	14.9	11.2

FLAME PATTERNS

Fuel/Air Ratio

Velocity - ft./sec.	.004	.008	.012	.016	.020
70	All blue except for a few yellow flashes in bottom half of chamber.	All yellow.	Yellow with narrow blue inner and outer fringes all around.	Bright yellow with very narrow blue inner and outer fringes all around. Small amount of flame through turbine annulus.	Bright yellow with very narrow blue inner and outer fringes all around. Considerable amount of flame through turbine annulus.
80	All blue except for a few yellow flashes in bottom half of chamber.	Yellow with very little blue intermixed all around.	Yellow and blue intermixed with a blue inner fringe all around	Yellow and blue intermixed with blue inner and outer fringes all around. No flame through turbine annulus.	Bright yellow with very narrow blue inner and outer fringes all around. Some flame through turbine annulus.
90	All blue with very occasional yellow flashes. Base plate red at bottom.	Mostly blue with a yellow spot at outlet of each vaporizer tube.	Yellow and blue intermixed with blue inner and outer fringes all around.	Yellow and blue intermixed with blue inner and outer fringes all around.	Yellow and blue intermixed with blue inner and outer fringes all around. Very little flame through turbine annulus.
100	All blue with very occasional yellow flashes.	Mostly blue with a yellow spot at outlet of each vaporizer tube.	Yellow and blue intermixed with blue inner and outer fringes all around.	Yellow and blue intermixed with blue inner and outer fringes all around.	Yellow and blue intermixed with blue inner and outer fringes all around. No flame through turbine annulus.
110		Mostly blue with a yellow spot at outlet of each vaporizer tube.	Yellow and blue intermixed with blue inner and outer fringes all around.	Yellow and blue intermixed all around.	

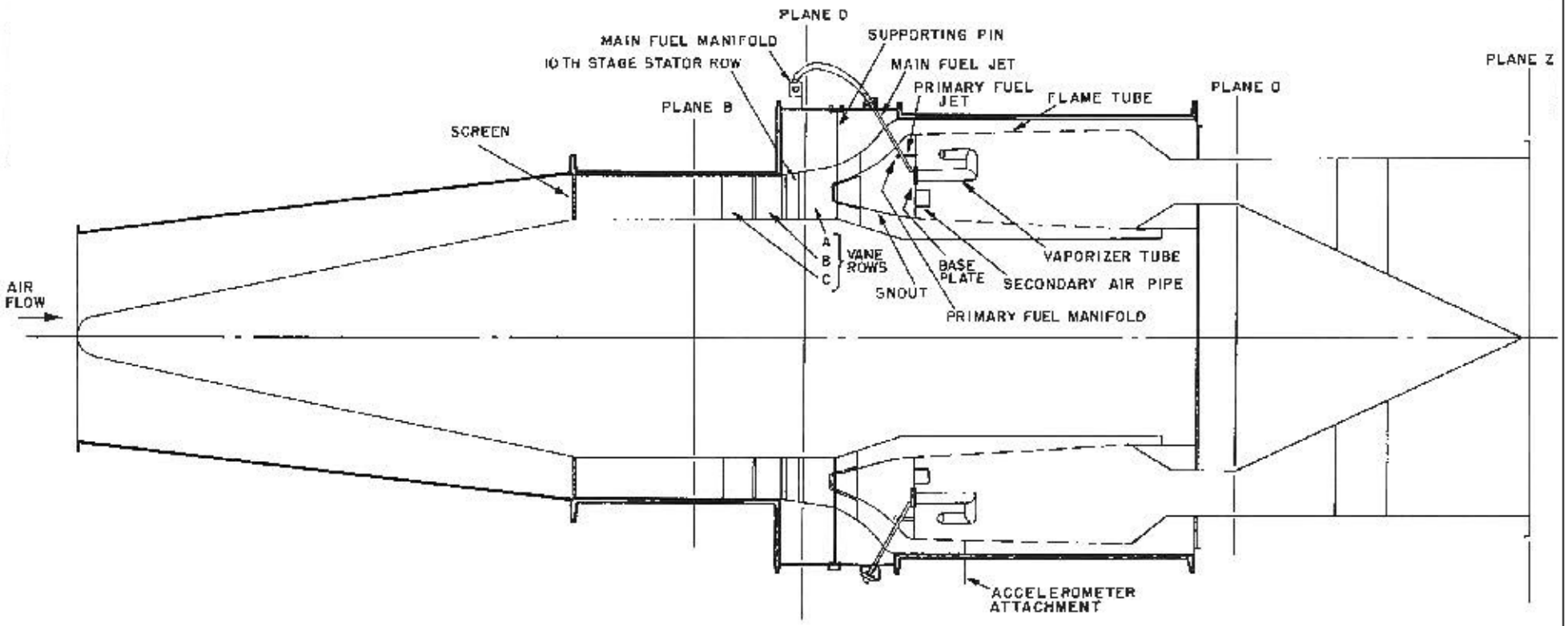

DIAGRAMMATIC LONGITUDINAL SECTION THROUGH PS. 13 ANNULAR VAPORIZING COMBUSTOR

FIG. 1
LR-154

FLAME TUBE OF P.S. 13 ANNULAR VAPORIZING COMBUSTOR

FIG. 3
LR-154

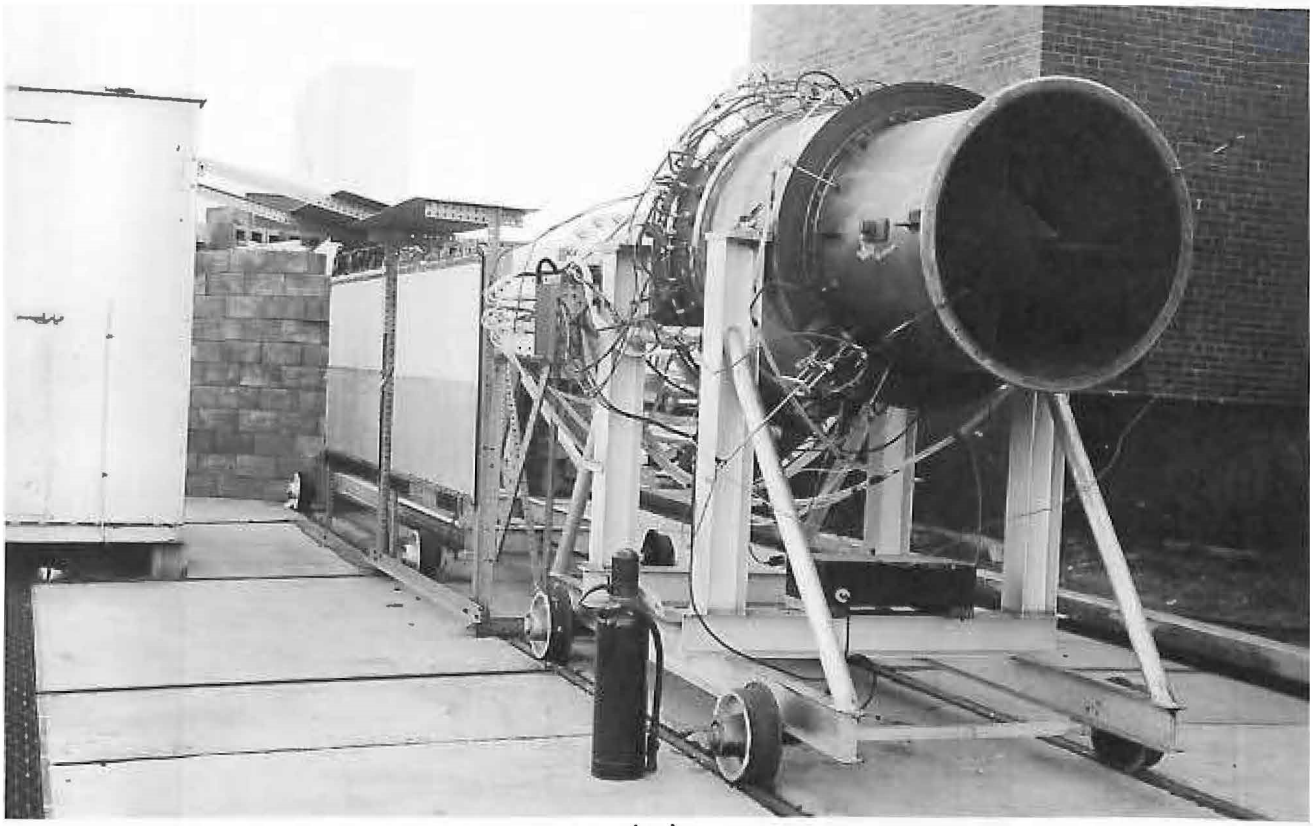

(a)

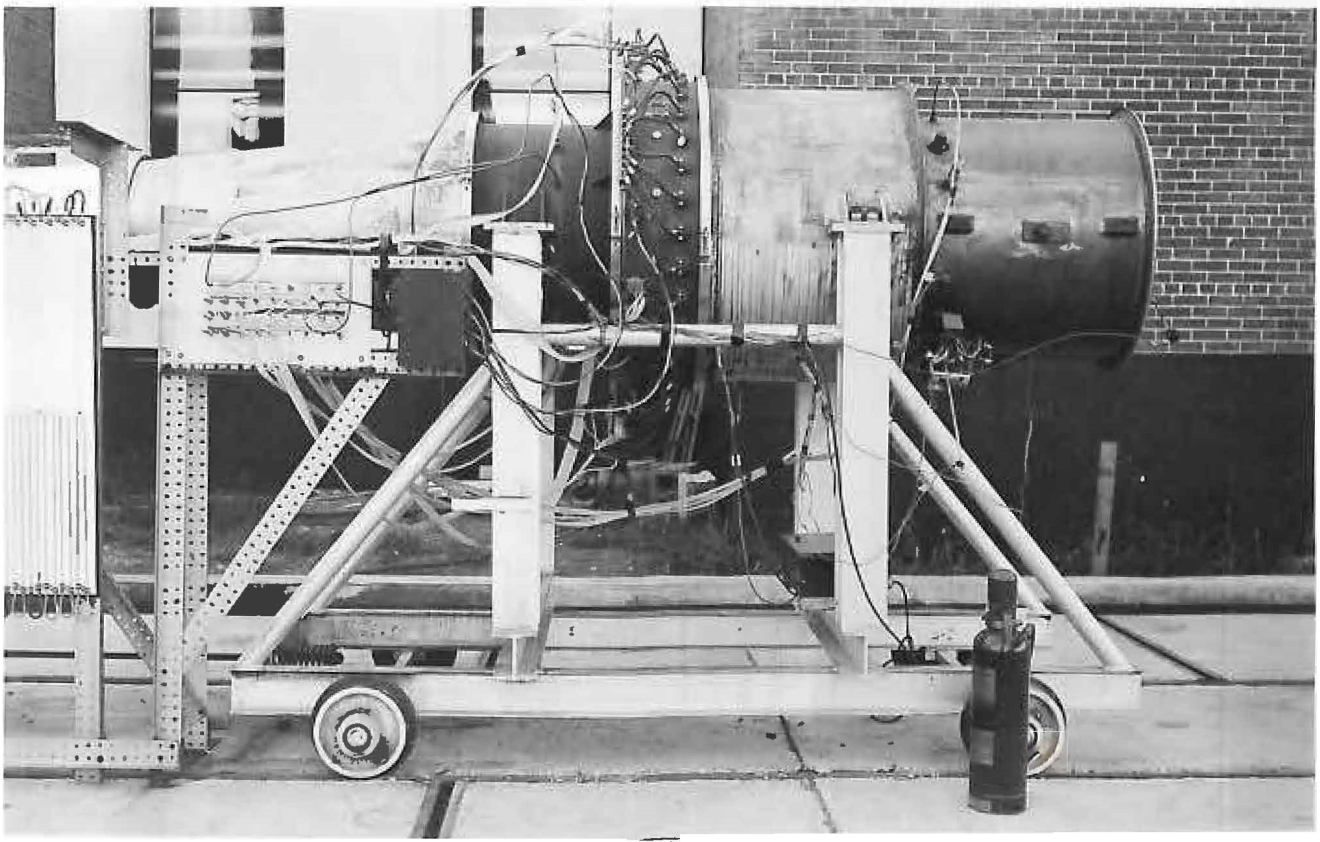

(b)

P.S. 13 ANNULAR VAPORIZING COMBUSTOR
ATMOSPHERIC PRESSURE TEST RIG WITH INSTRUMENTATION INSTALLED

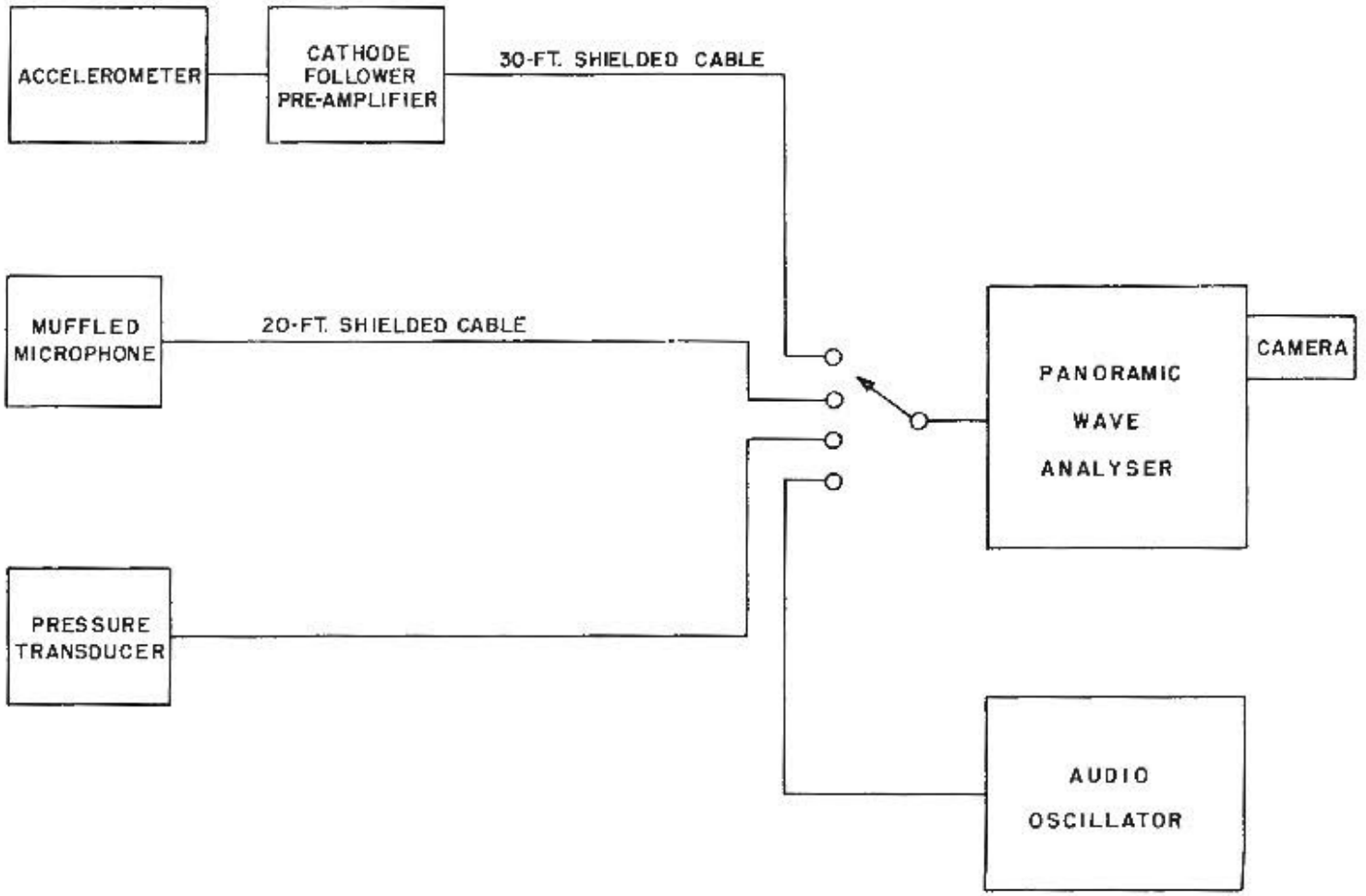

BLOCK DIAGRAM OF COMBUSTION ROUGHNESS ANALYSING EQUIPMENT

FIG. 4
LR-154

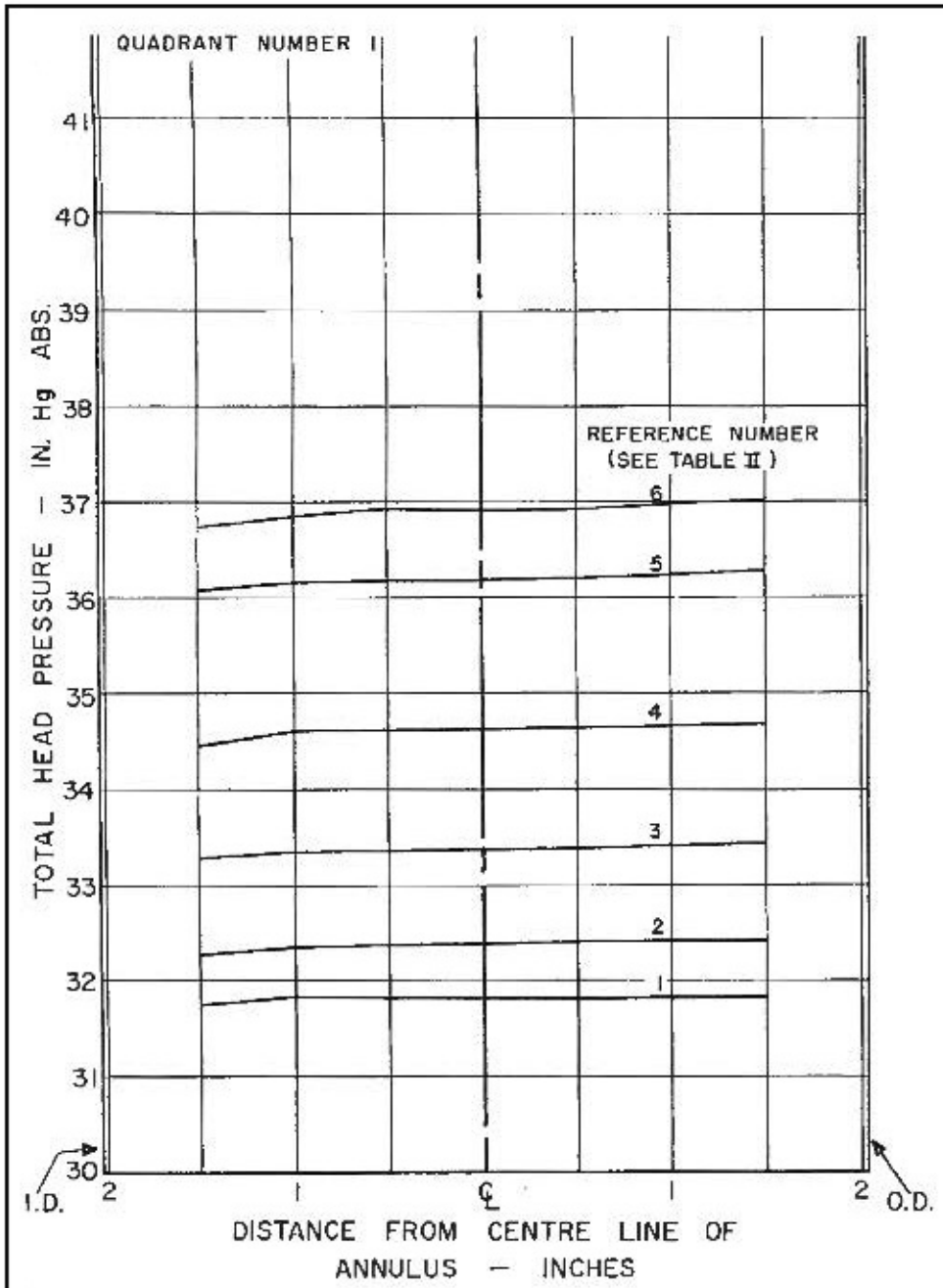

TOTAL HEAD PRESSURE DISTRIBUTIONS,
PLANE B, SCREEN IN PLACE

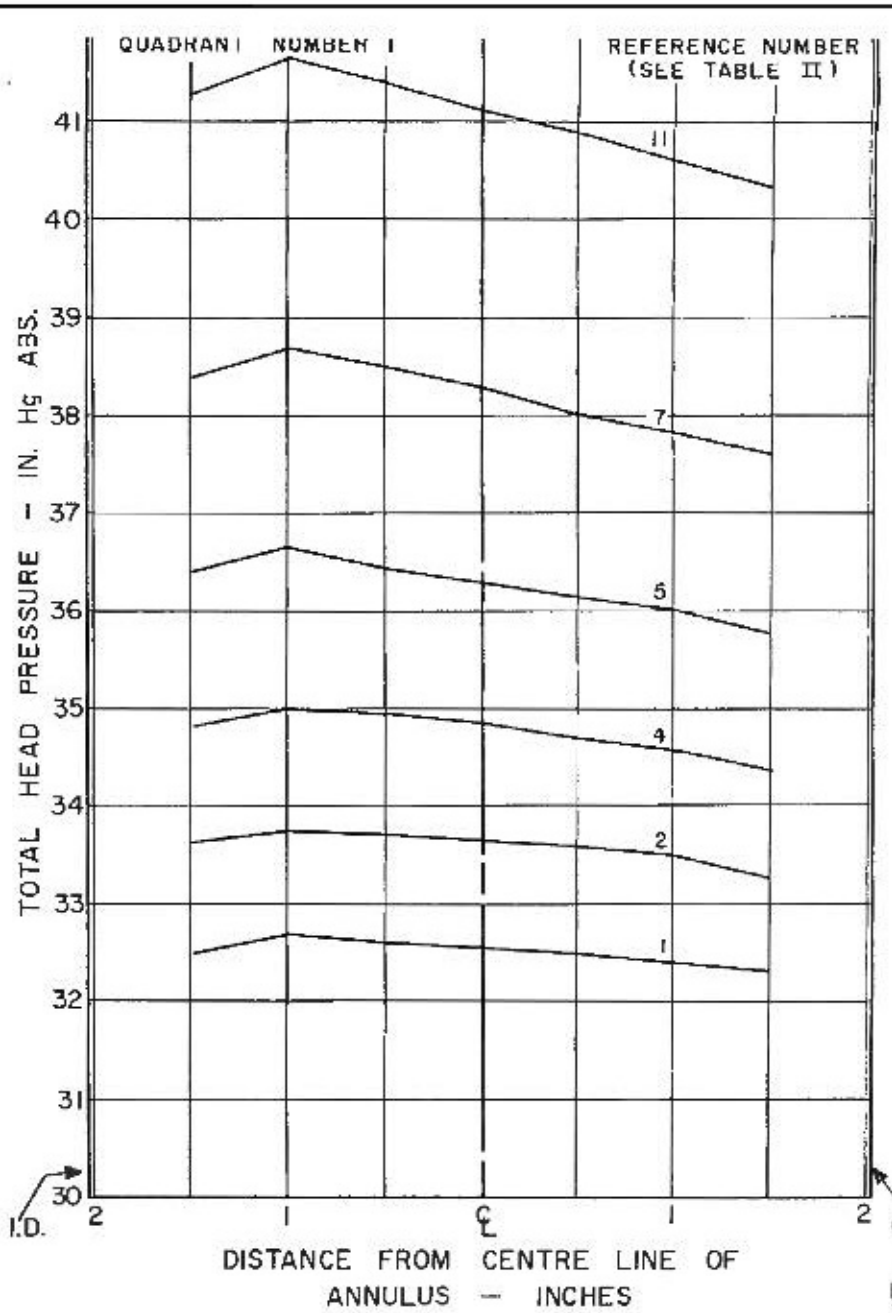

TOTAL HEAD PRESSURE DISTRIBUTIONS,
PLANE B, SCREEN REMOVED

FIG. 5a
LR-154

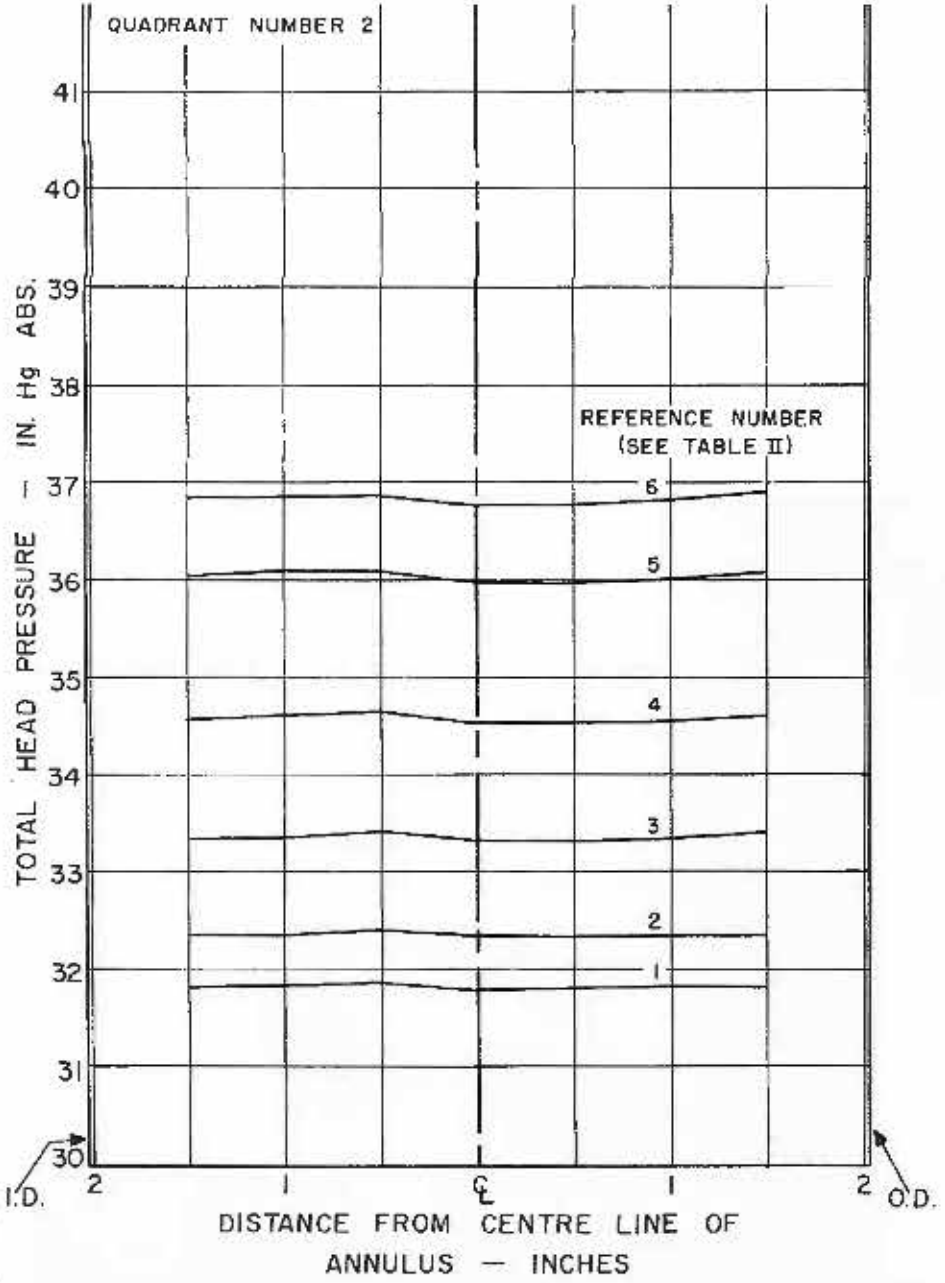

TOTAL HEAD PRESSURE DISTRIBUTIONS,
PLANE B, SCREEN IN PLACE

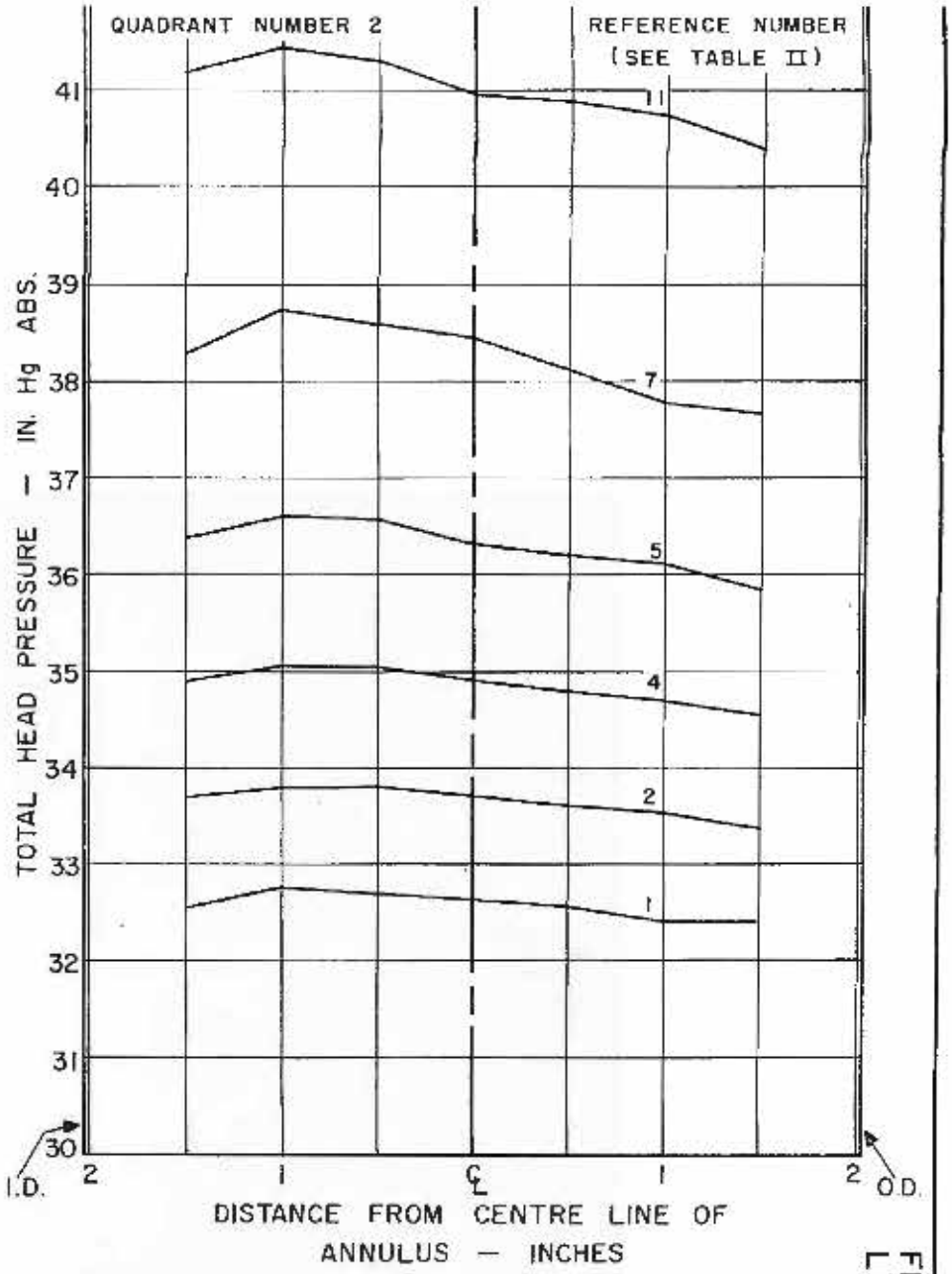

TOTAL HEAD PRESSURE DISTRIBUTIONS,
PLANE B, SCREEN REMOVED

FIG. 5b
LR - 154

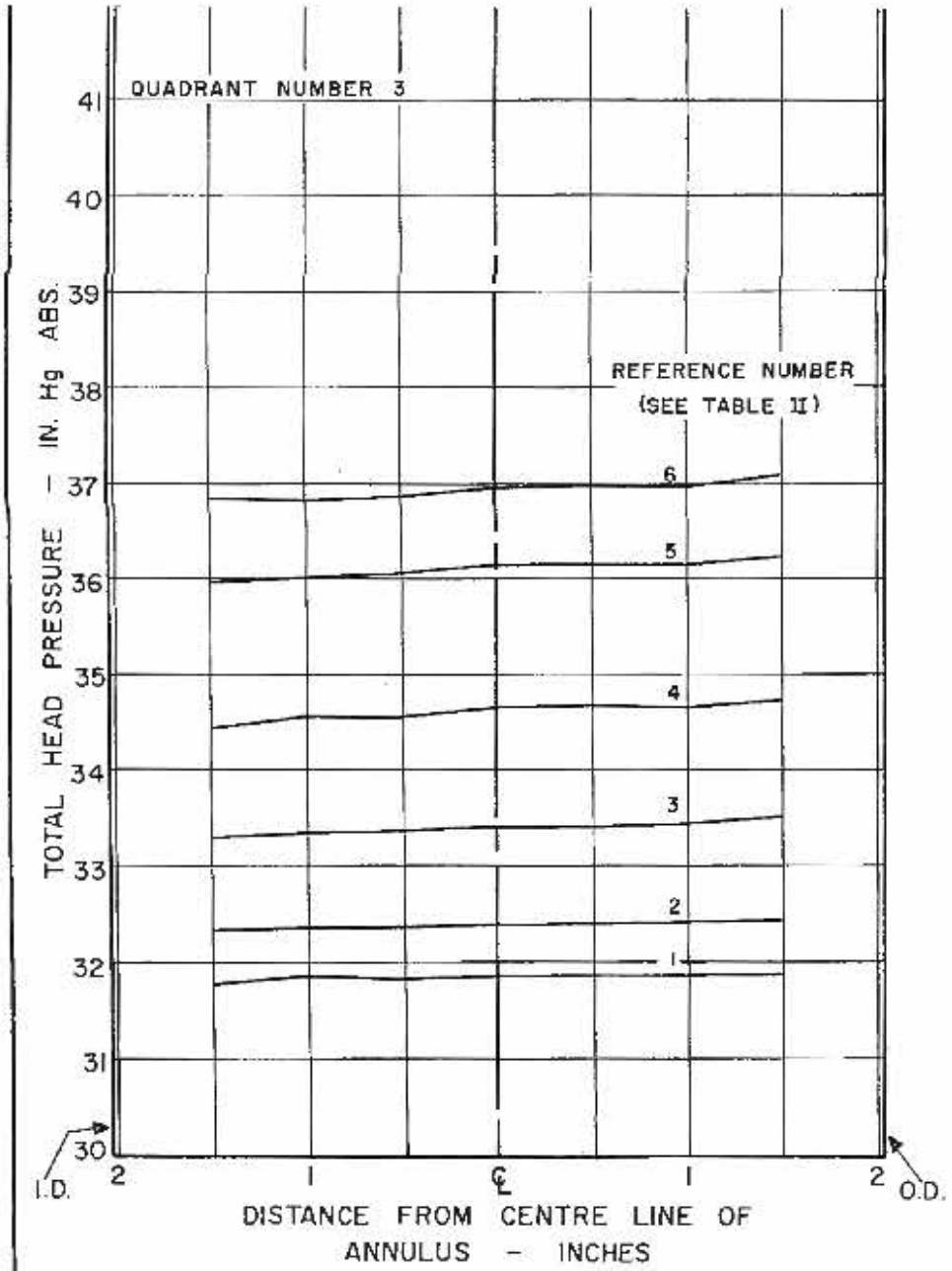

TOTAL HEAD PRESSURE DISTRIBUTIONS,
PLANE B, SCREEN IN PLACE

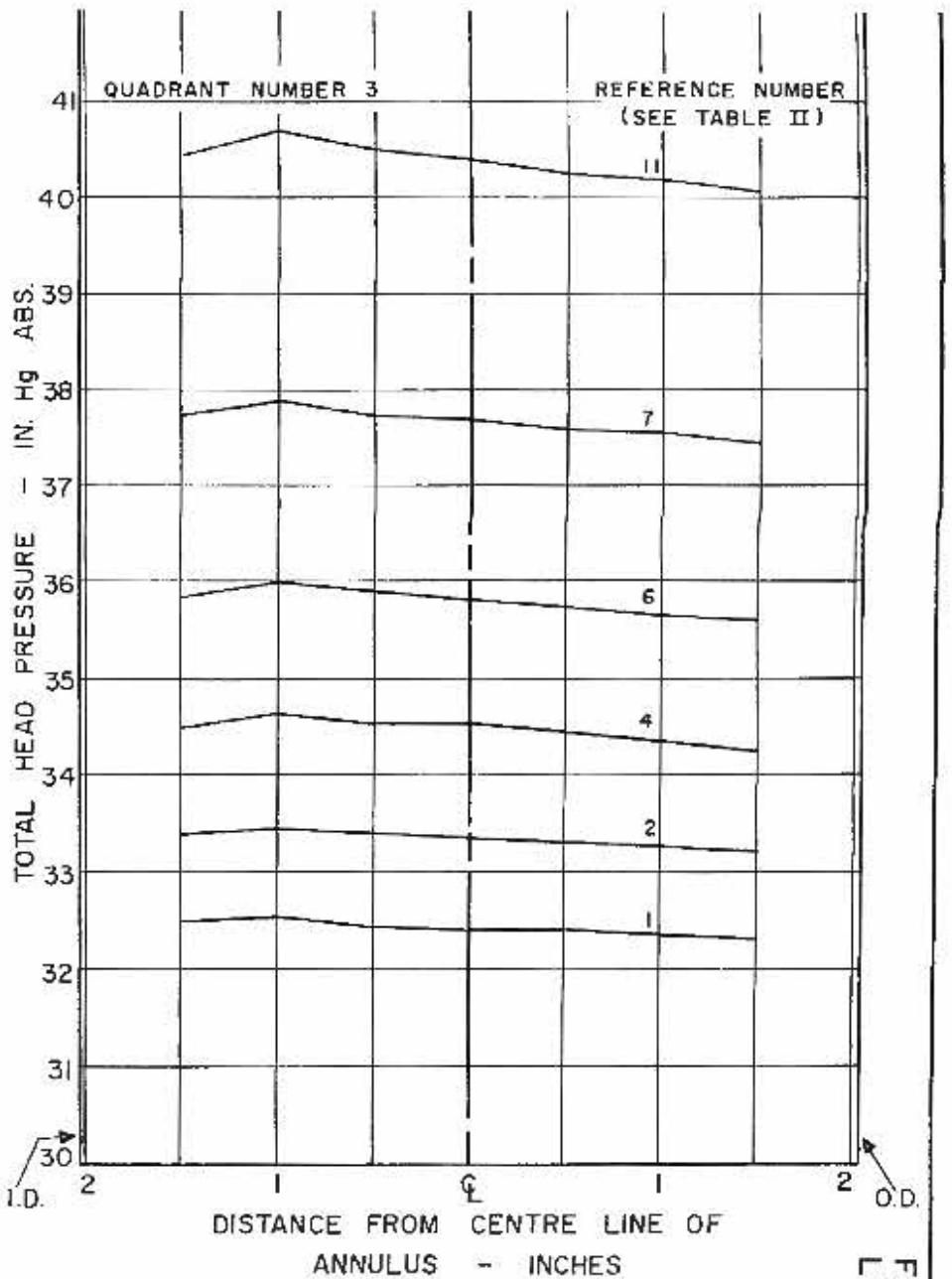

TOTAL HEAD PRESSURE DISTRIBUTIONS,
PLANE B, SCREEN REMOVED

FIG. 5c
LR - 154

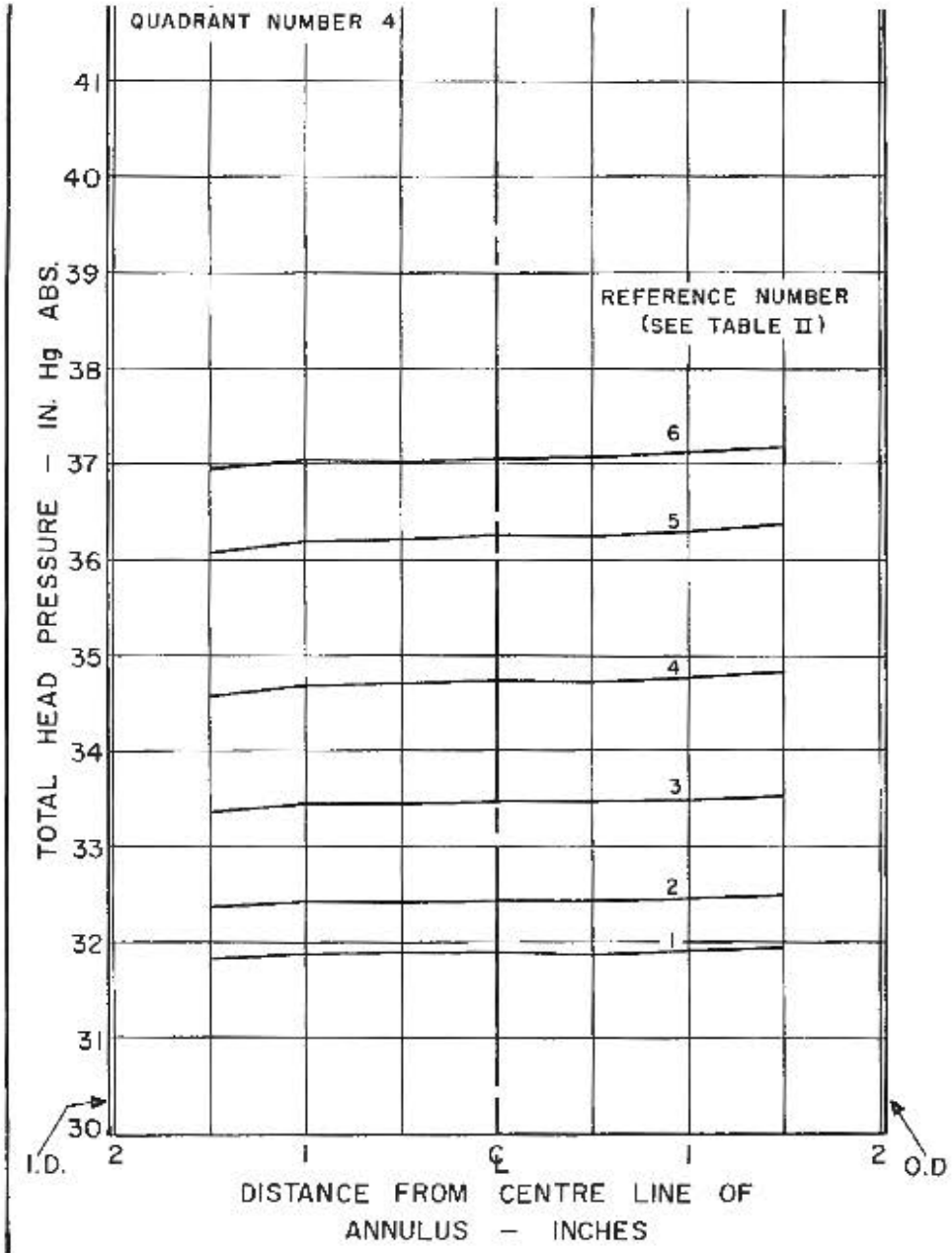

TOTAL HEAD PRESSURE DISTRIBUTIONS,
PLANE B, SCREEN IN PLACE

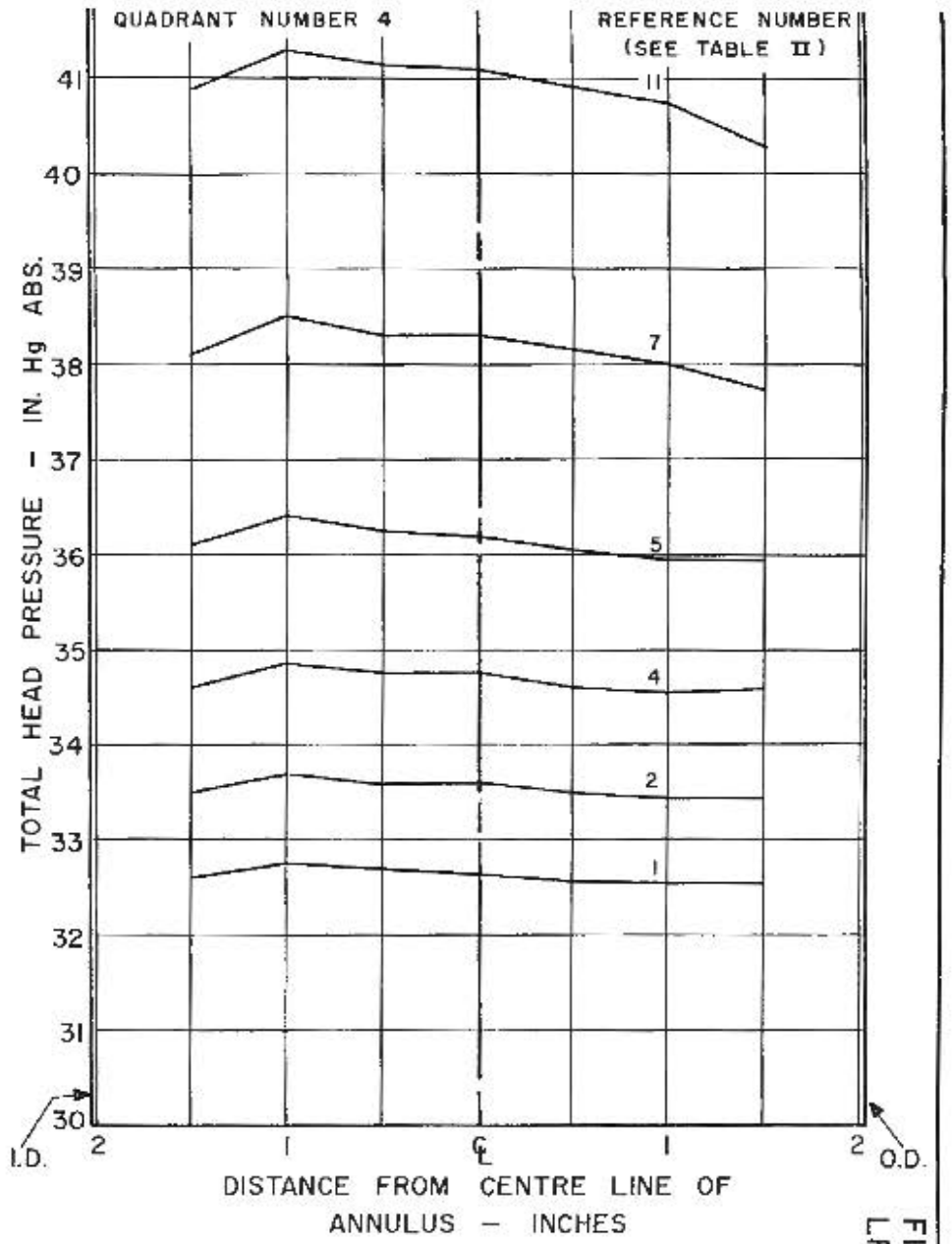

TOTAL HEAD PRESSURE DISTRIBUTIONS,
PLANE B, SCREEN REMOVED

FIG. 5d
LR - 154

FIG. 6
LR-154

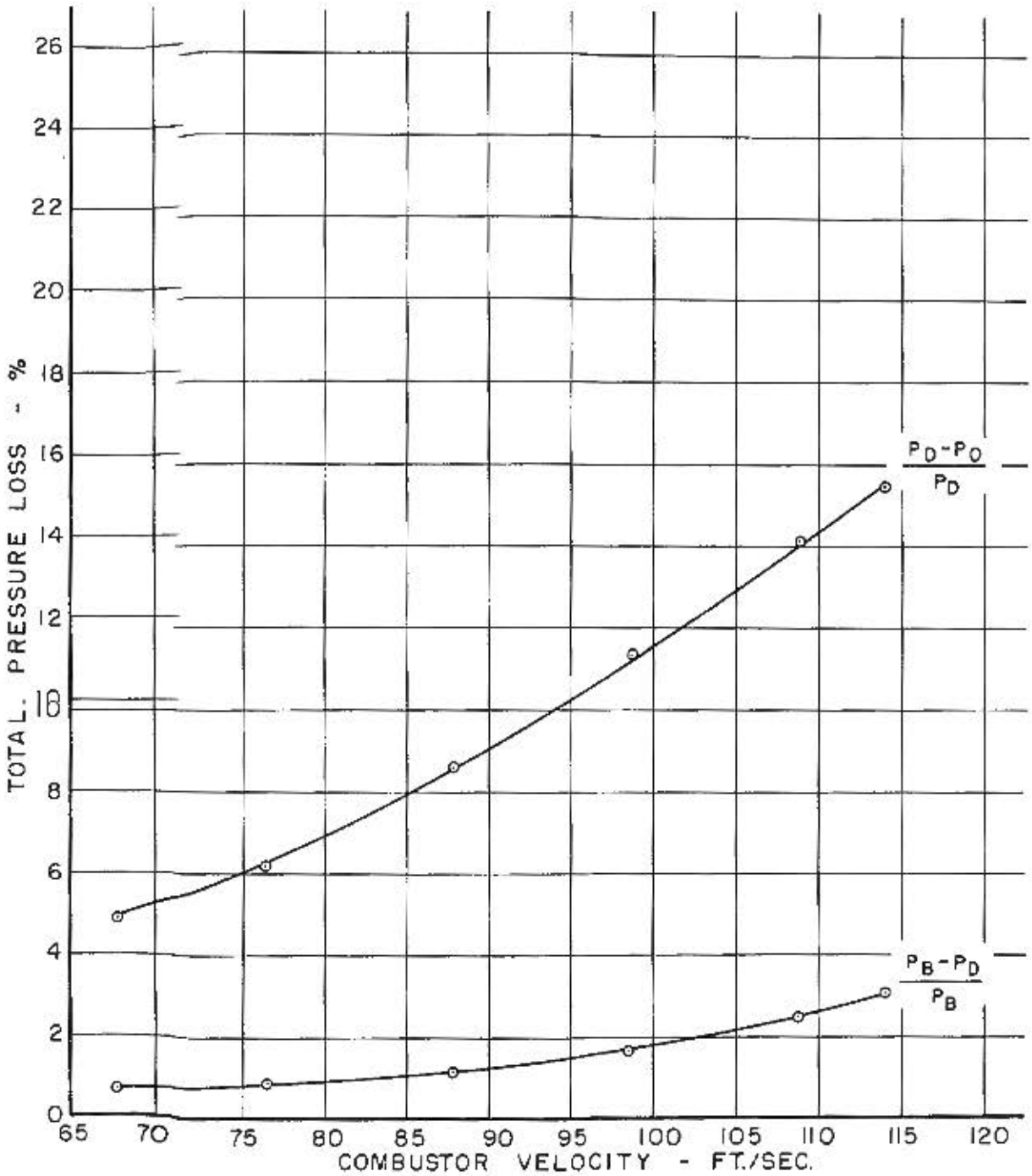

TOTAL PRESSURE LOSS BETWEEN PLANES B AND D AND BETWEEN PLANES D AND O AS A PERCENTAGE OF THE INLET PRESSURE IN EACH CASE:

SCREEN IN PLACE

FIG. 7
LR-154

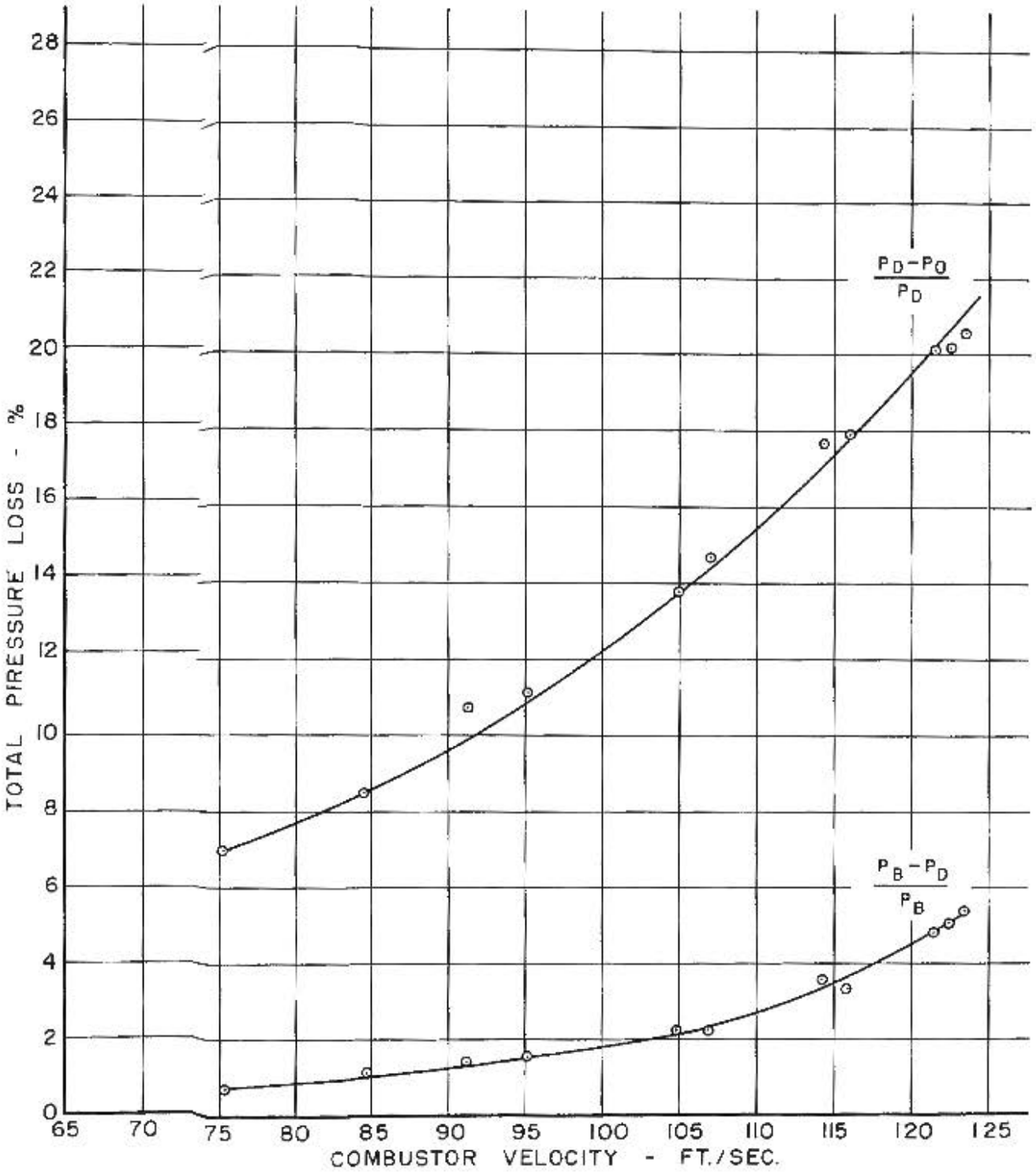

TOTAL PRESSURE LOSS BETWEEN PLANES B AND D AND BETWEEN PLANES D AND O AS A PERCENTAGE OF THE INLET PRESSURE IN EACH CASE:

SCREEN REMOVED

FIG. 8
LR-154

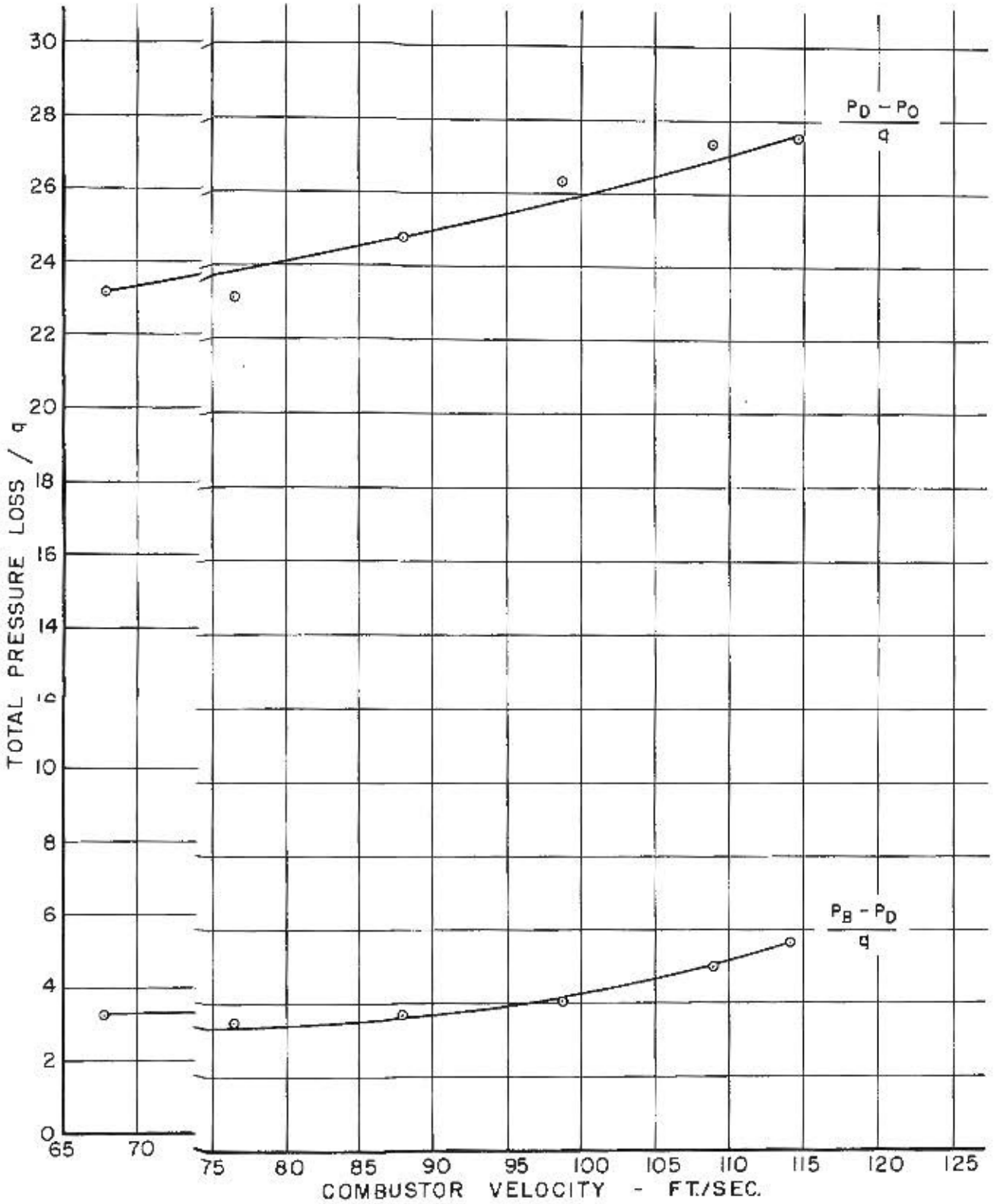

TOTAL PRESSURE LOSS BETWEEN PLANES B AND D AND BETWEEN PLANES D AND O (SCREEN IN PLACE) IN TERMS OF COMBUSTOR NOMINAL q WHERE:

$q = \frac{\rho V^2}{2}$

ρ = TOTAL DENSITY AT PLANE D
V = COMBUSTOR VELOCITY

FIG. 9
LR-154

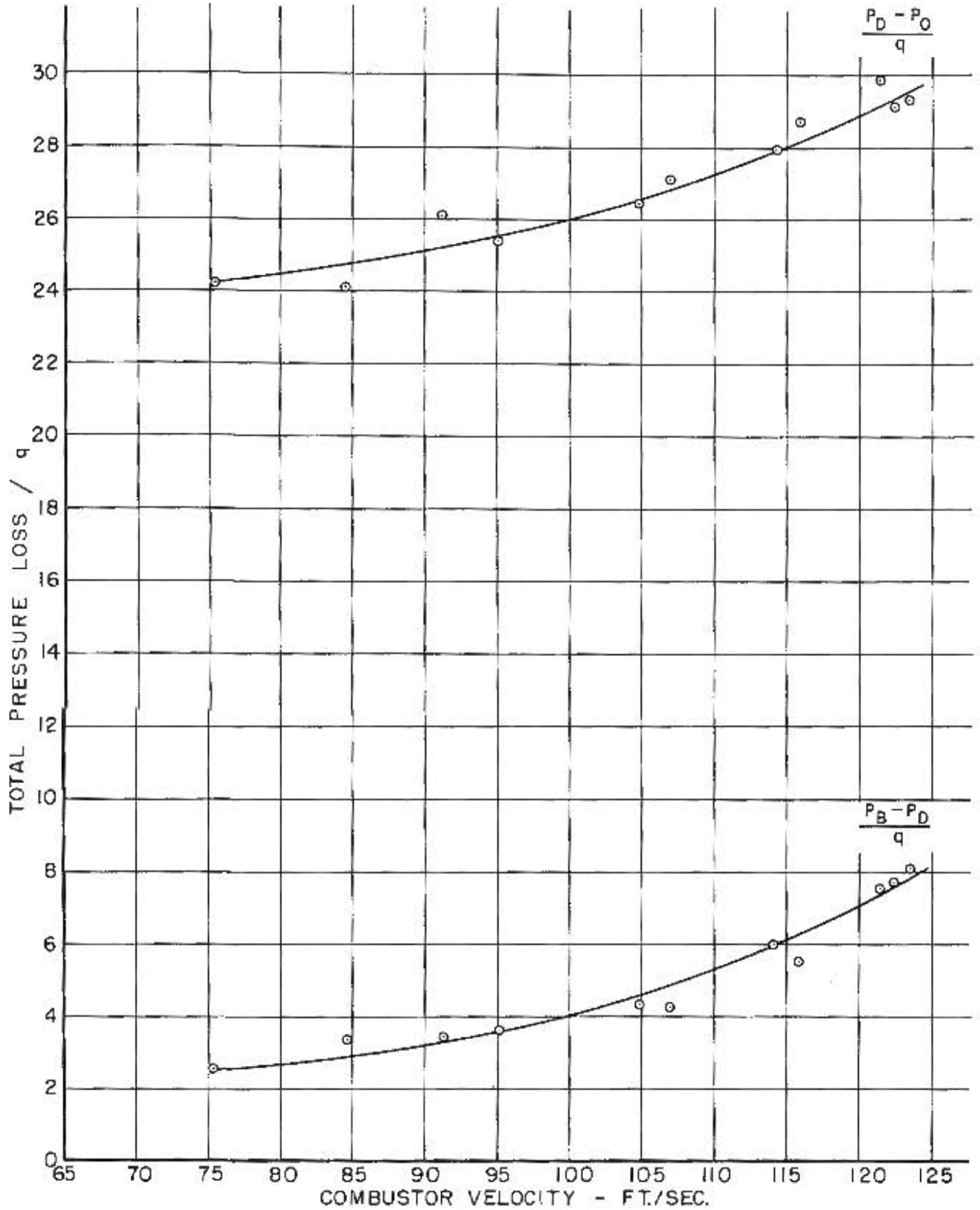

TOTAL PRESSURE LOSS BETWEEN PLANES B AND D AND BETWEEN PLANES D AND O (SCREEN REMOVED) IN TERMS OF COMBUSTOR NOMINAL q WHERE:

$q = \frac{\rho V^2}{2}$

ρ = TOTAL DENSITY AT PLANE D
V = COMBUSTOR VELOCITY

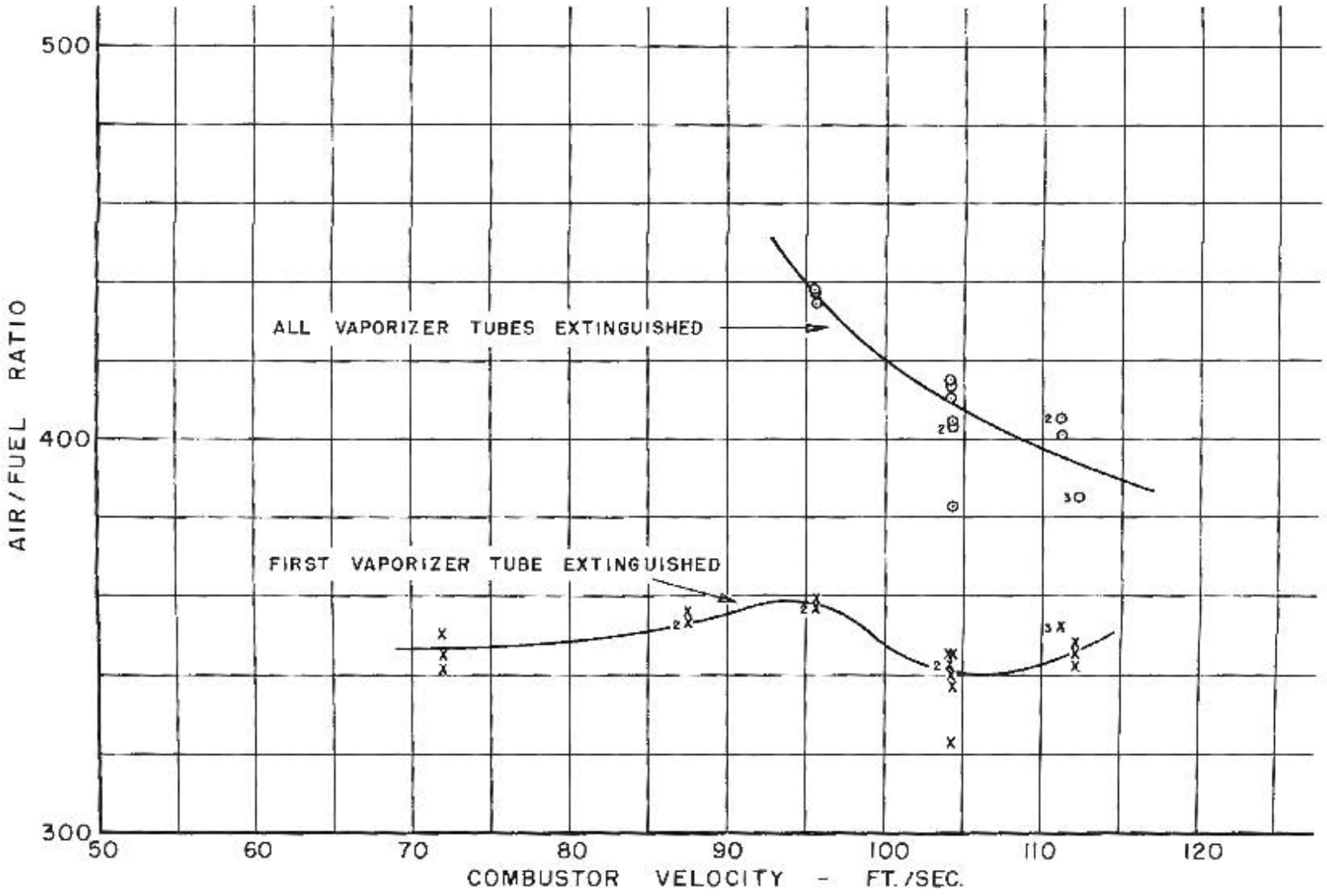

WEAK STABILITY LIMITS - SCREEN IN PLACE

(NUMBERS BESIDE POINTS INDICATE NUMBER OF TESTS RESULTING IN SAME POINT)

FIG. 10
LR-154

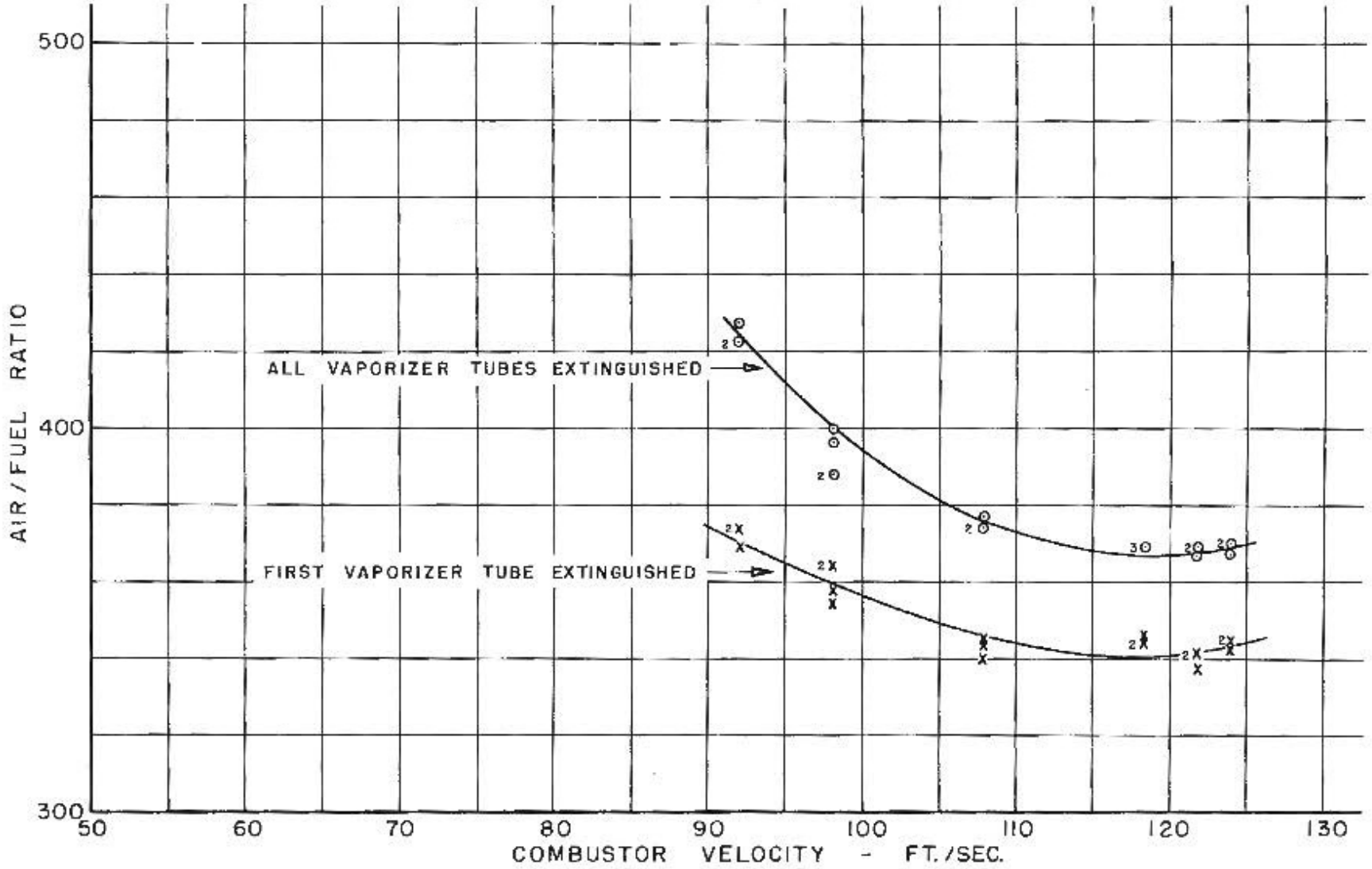

WEAK STABILITY LIMITS - SCREEN REMOVED

(NUMBERS BESIDE POINTS INDICATE NUMBER OF TESTS RESULTING IN SAME POINT)

FIG. 11
LR-154

FIG. 12,13
LR-154

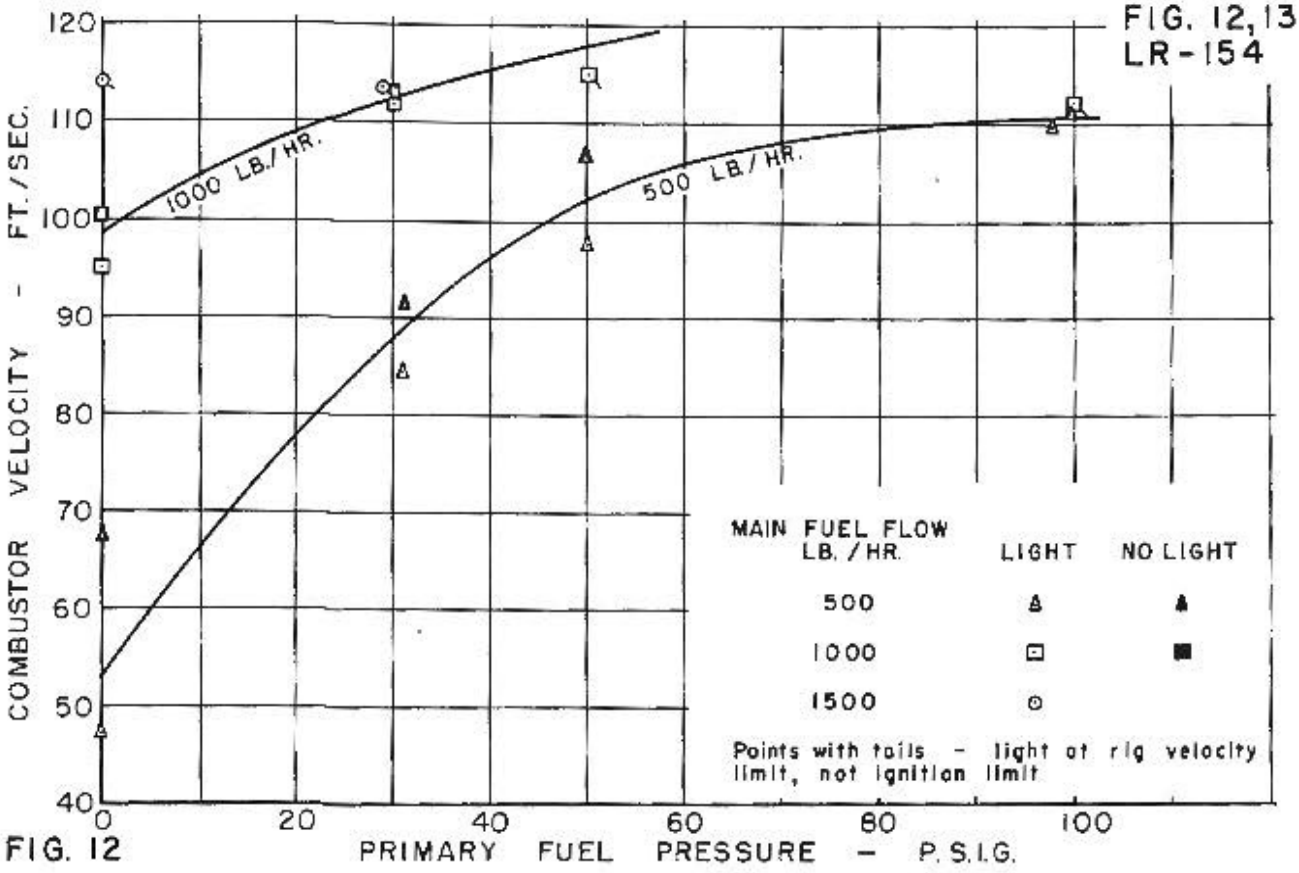

FIG. 12

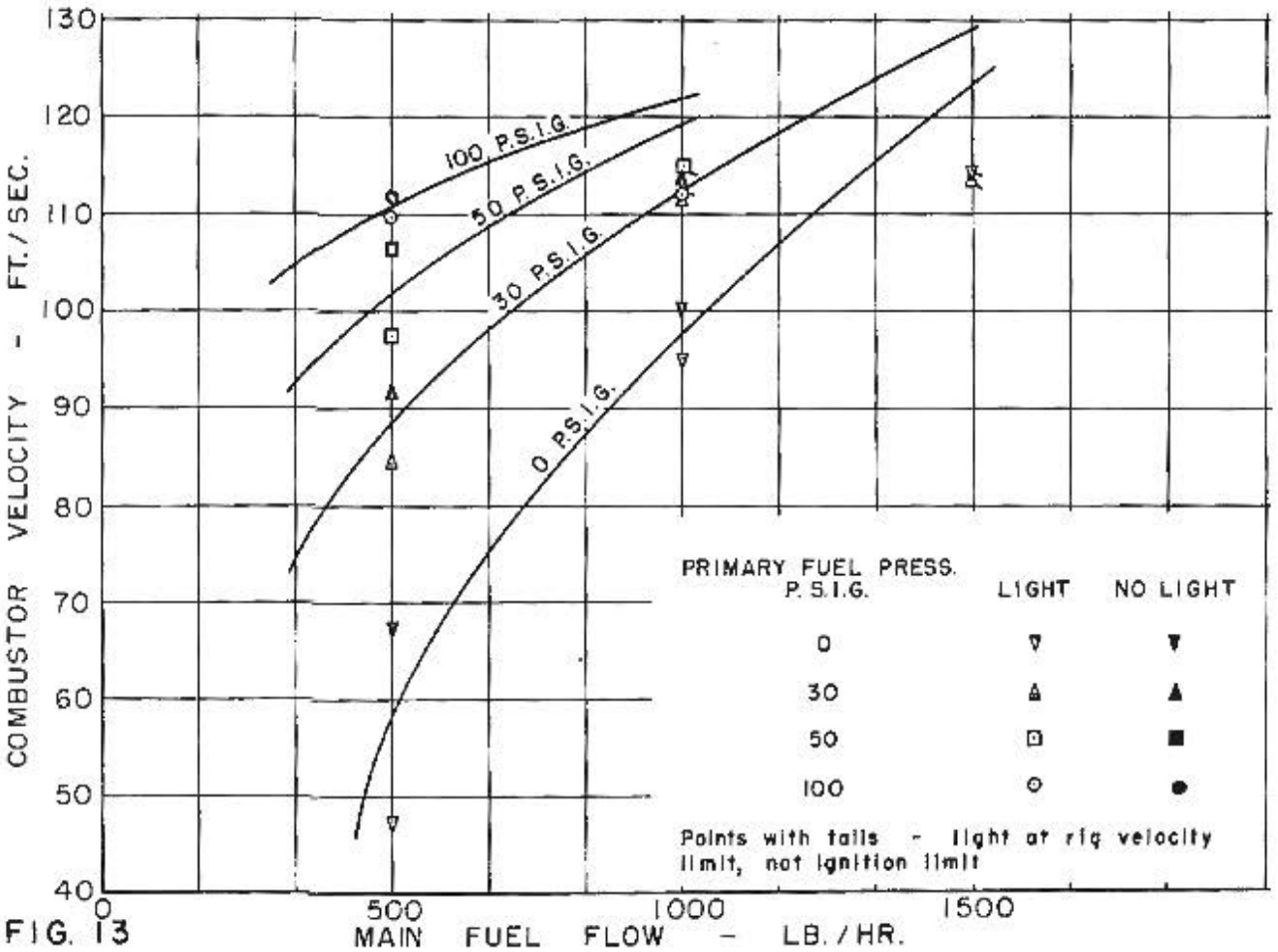

FIG. 13

WEAK IGNITION LIMITS - SCREEN IN PLACE

FIG. 14,15
LR-154

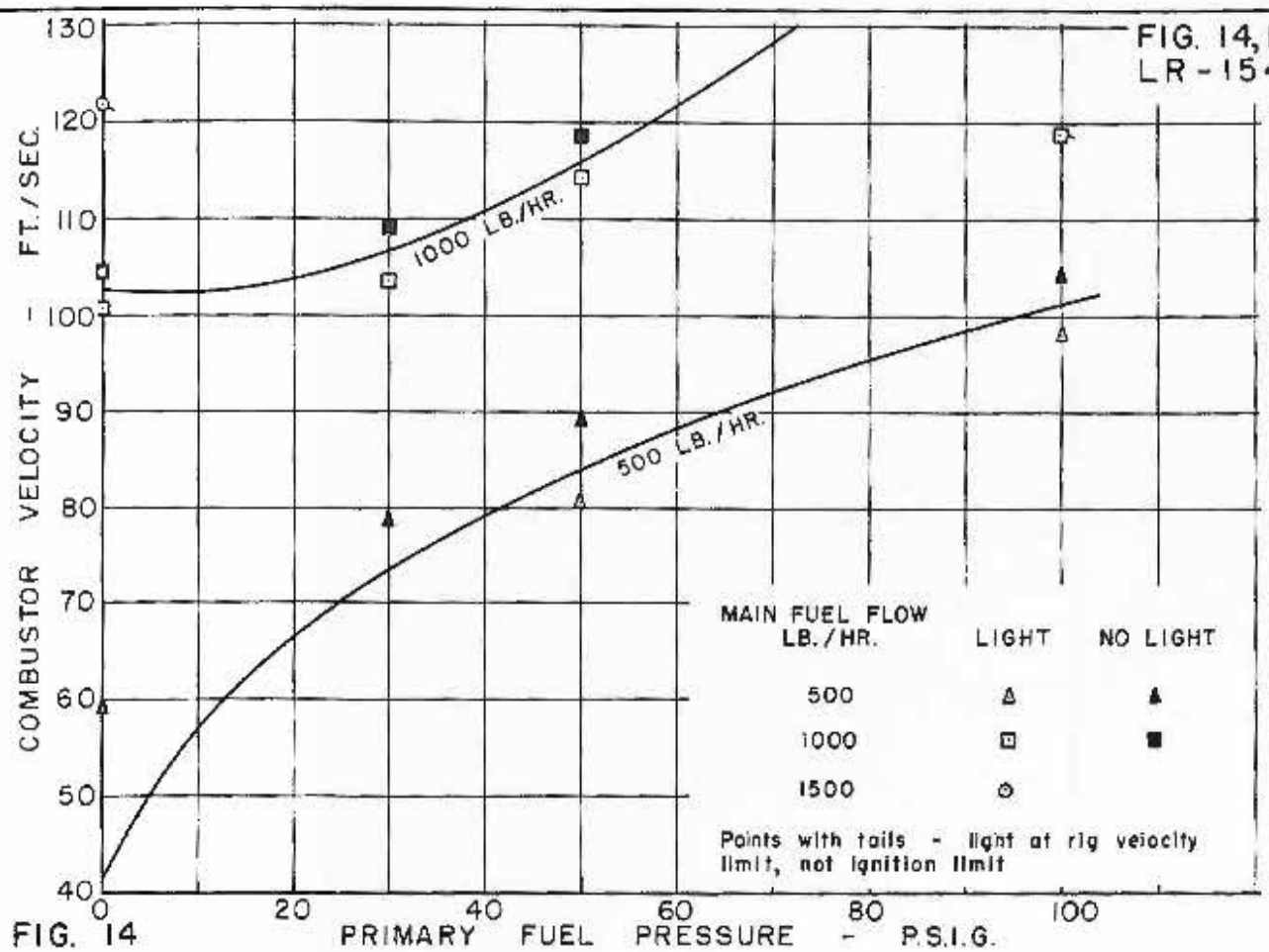

FIG. 14

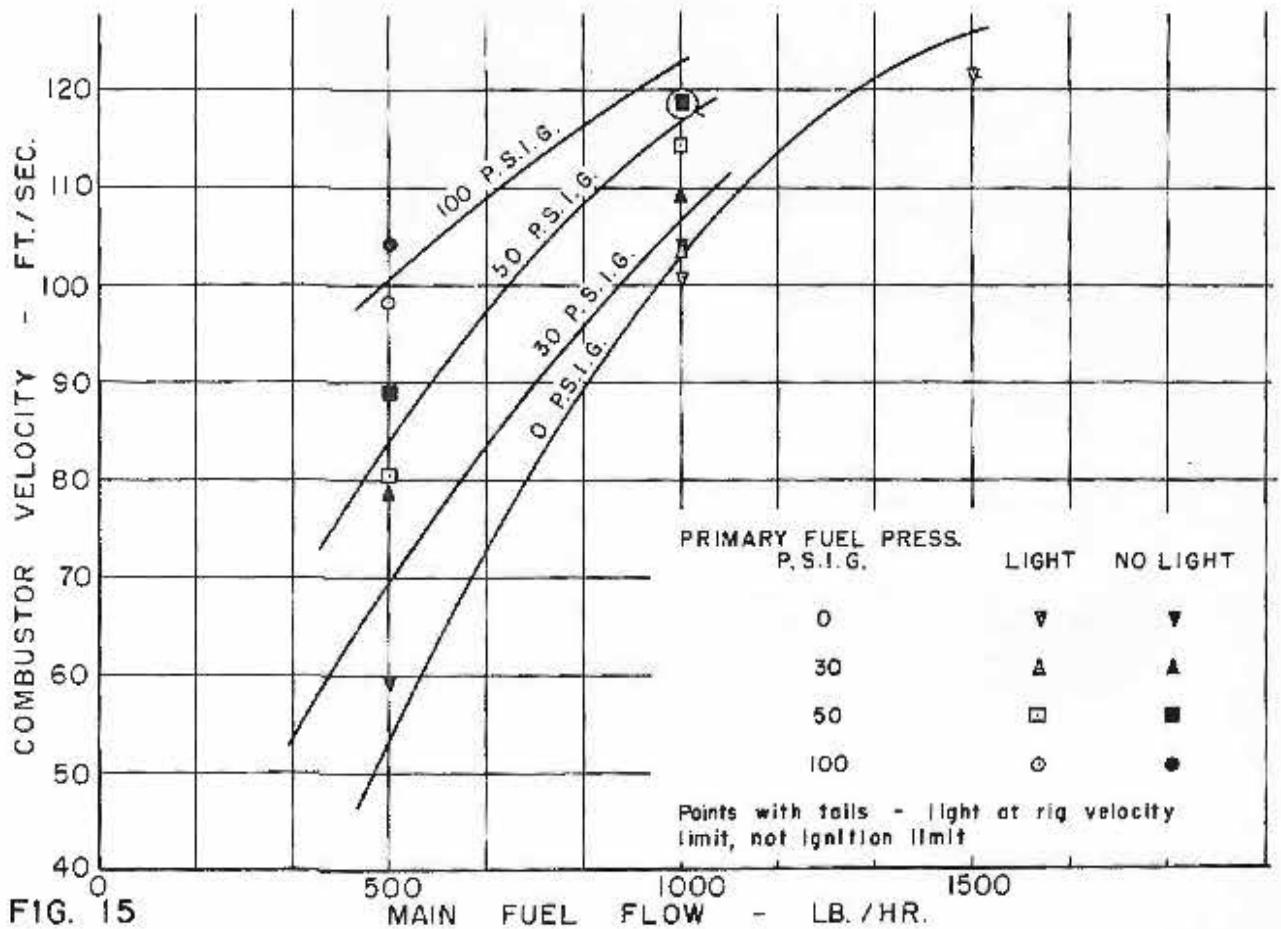

FIG. 15

WEAK IGNITION LIMITS - SCREEN REMOVED

FIG. 16
LR - 154

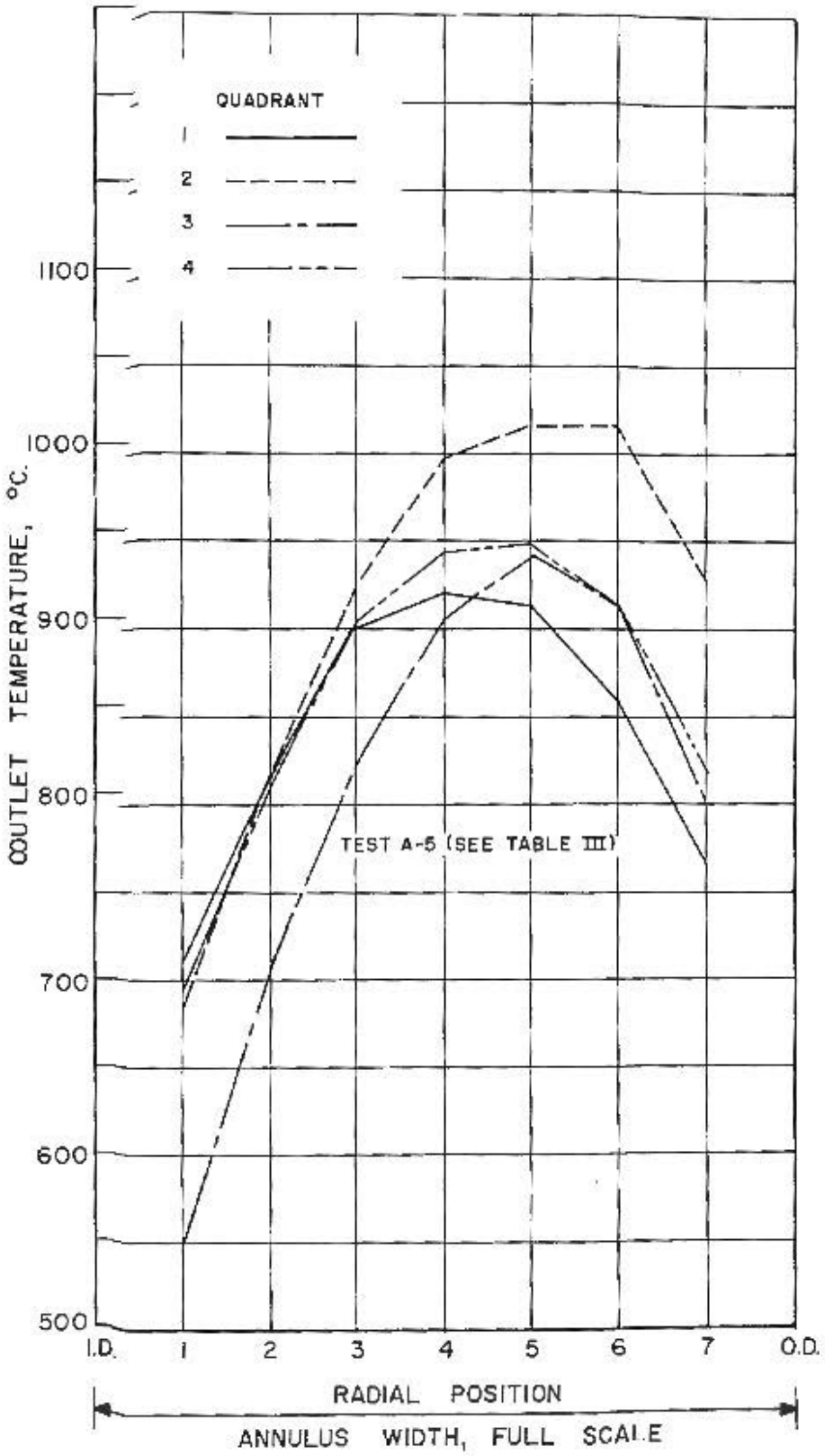

OUTLET TEMPERATURE DISTRIBUTION
NOMINAL VELOCITY = 70 FT./SEC.

FIG. 17
LR - 154

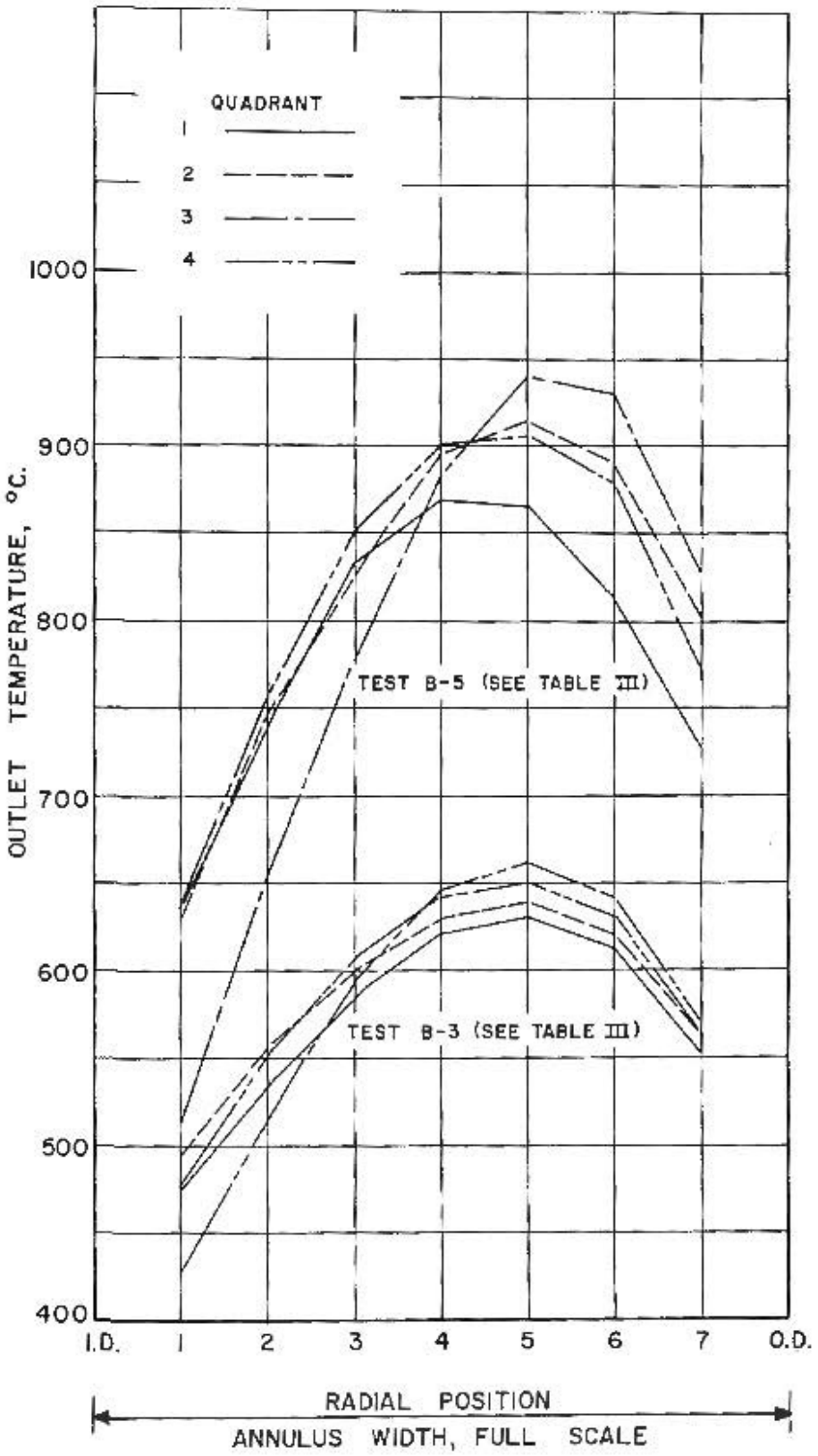

OUTLET TEMPERATURE DISTRIBUTION
NOMINAL VELOCITY = 80 FT./SEC.

FIG. 18
LR - 154

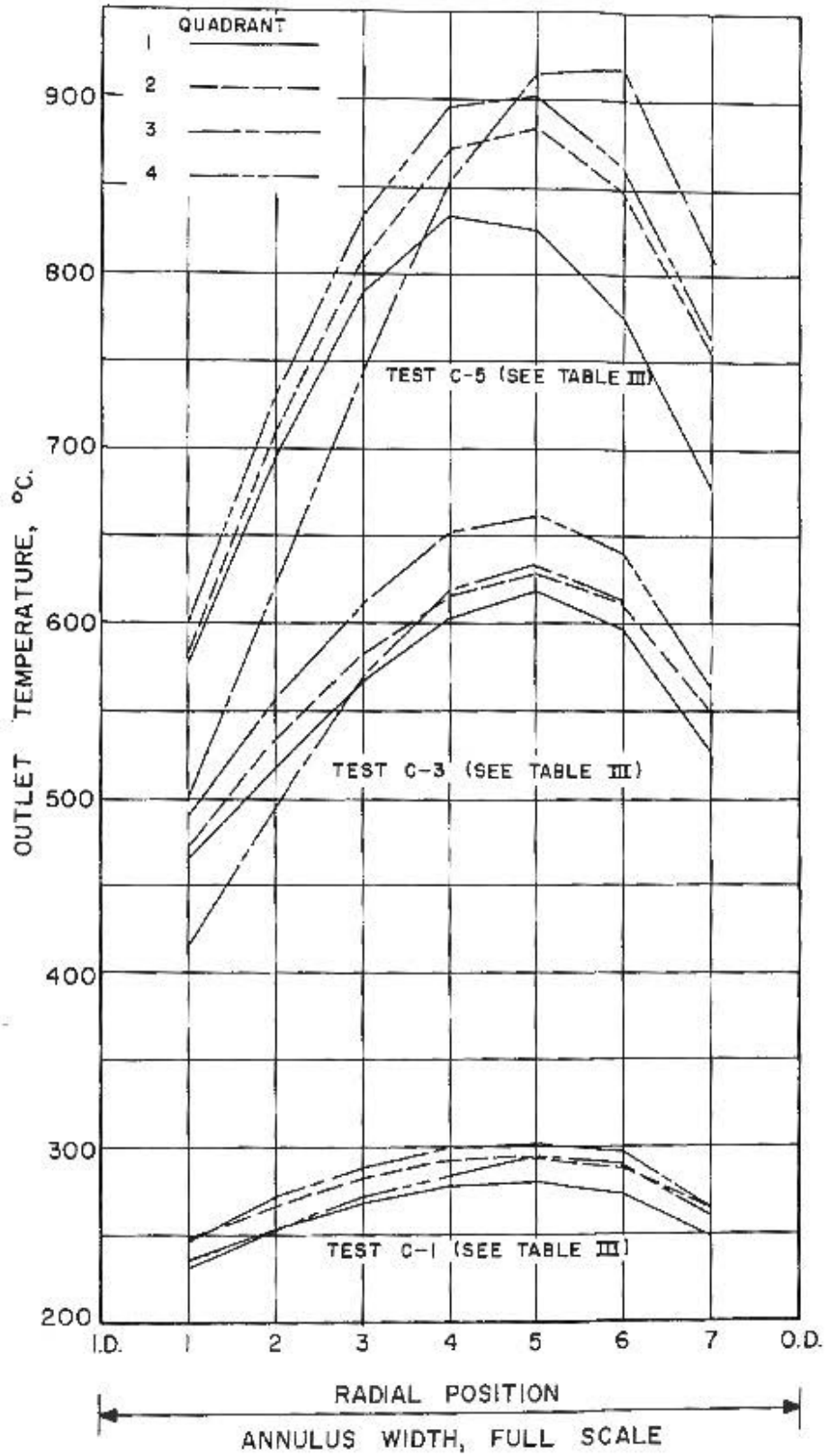

OUTLET TEMPERATURE DISTRIBUTION
NOMINAL VELOCITY = 90 FT./SEC.

FIG. 19
LR - 154

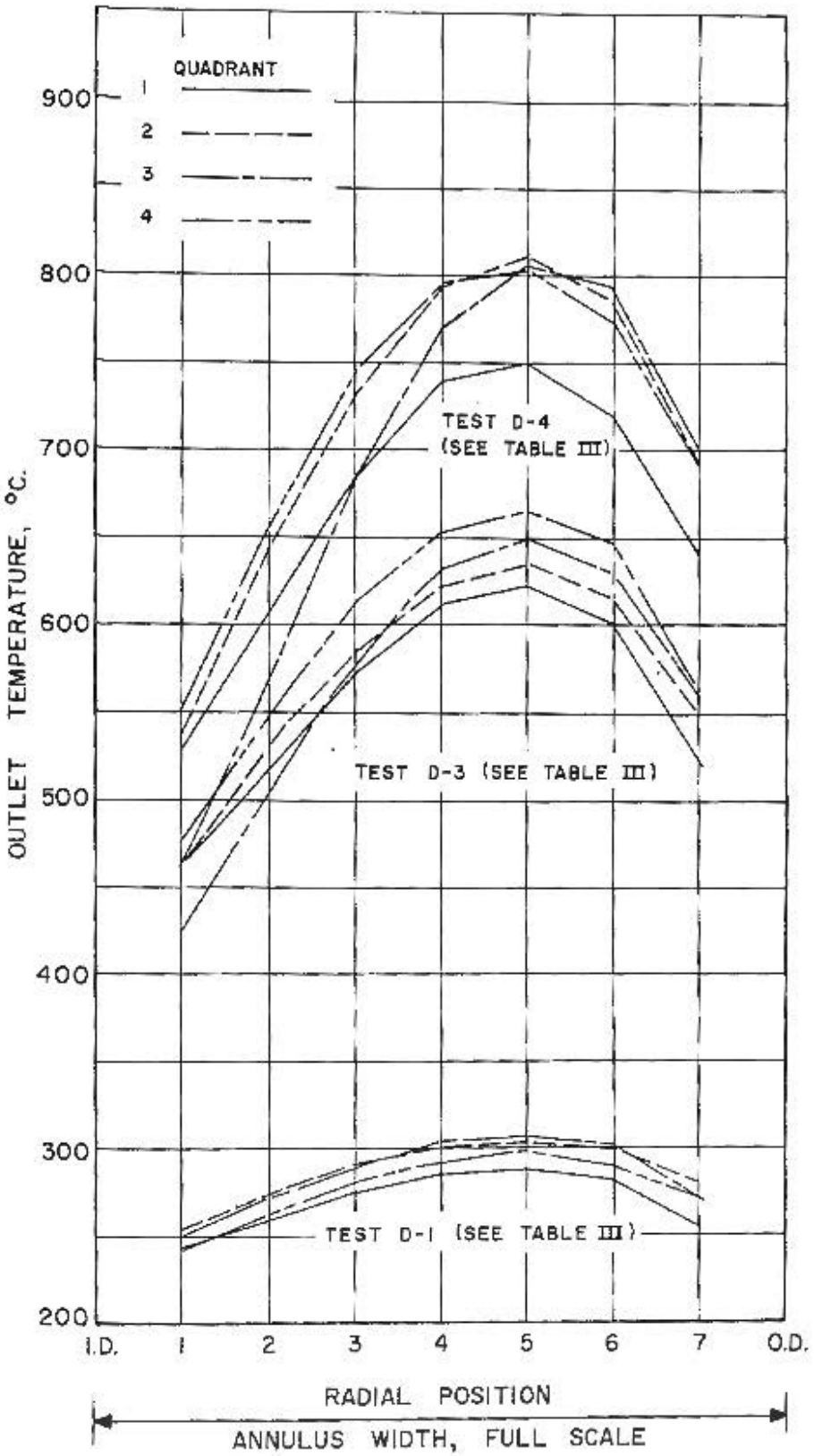

OUTLET TEMPERATURE DISTRIBUTION
NOMINAL VELOCITY = 100 FT./SEC.

FIG. 20
LR - 154

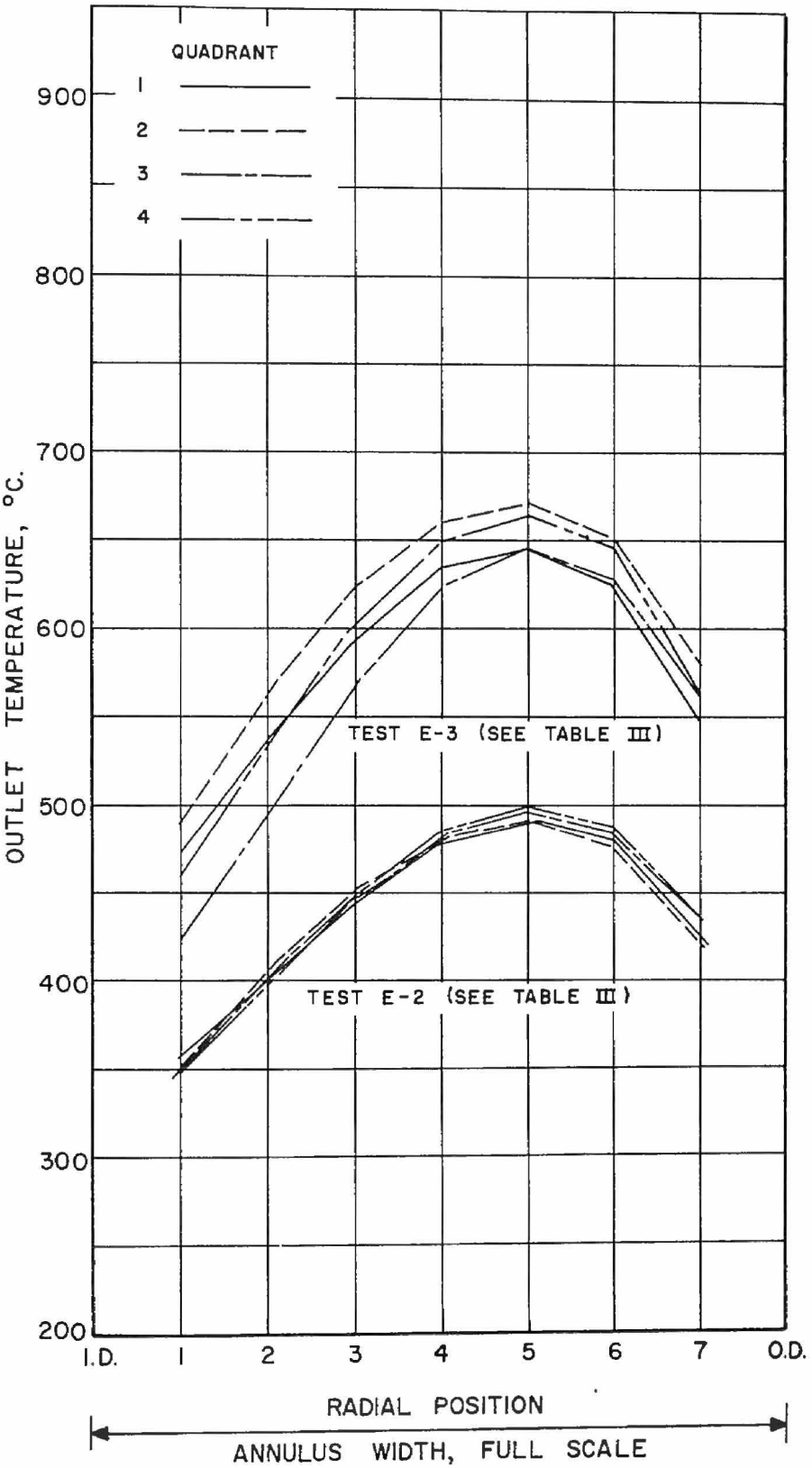

OUTLET TEMPERATURE DISTRIBUTION
NOMINAL VELOCITY = 110 FT./SEC.

FIG. 21
LR-154

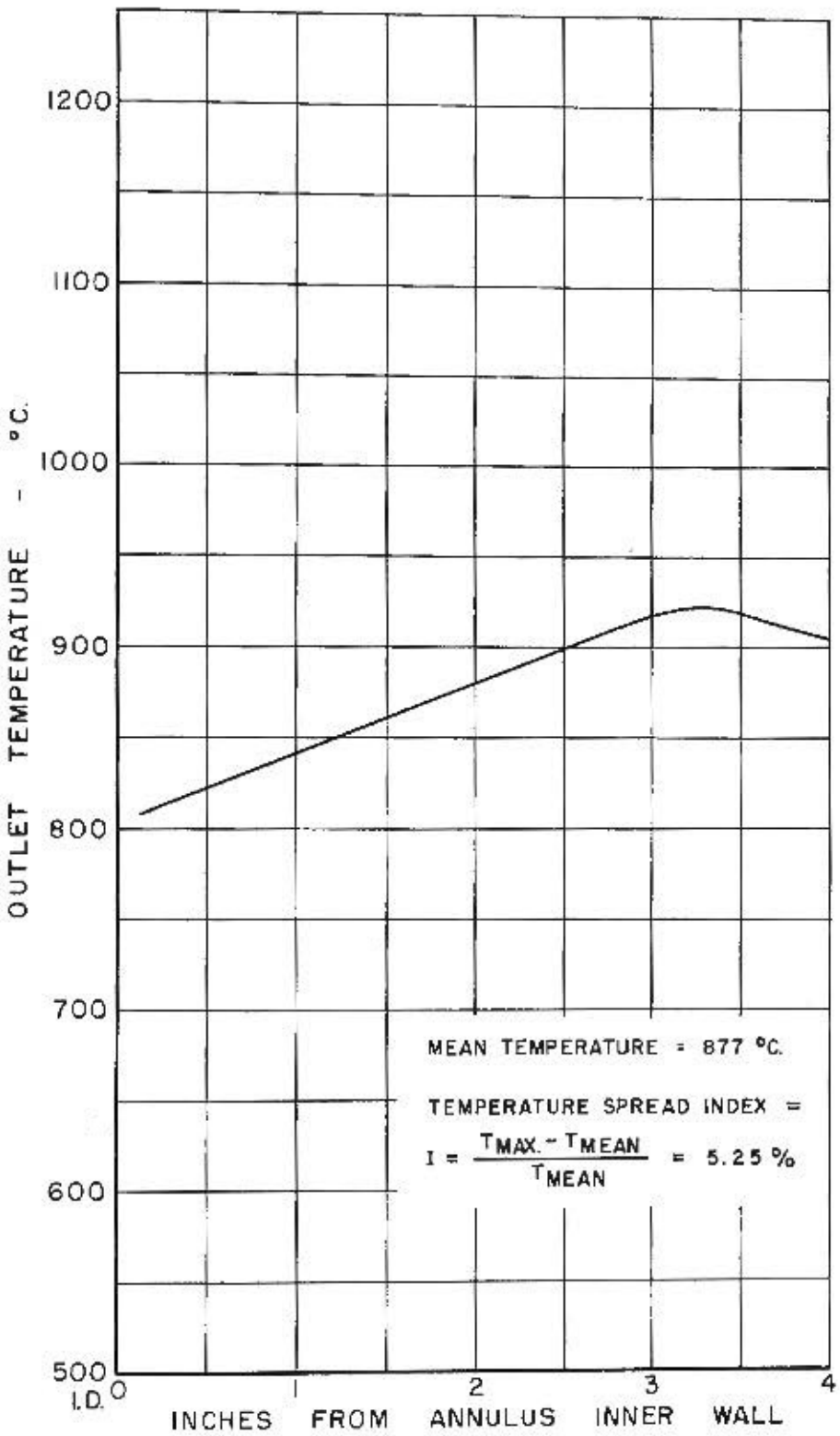

IDEAL OUTLET TEMPERATURE PROFILE
DATA SUPPLIED BY ORENDA ENGINES LIMITED

FIG. 22
LR-154

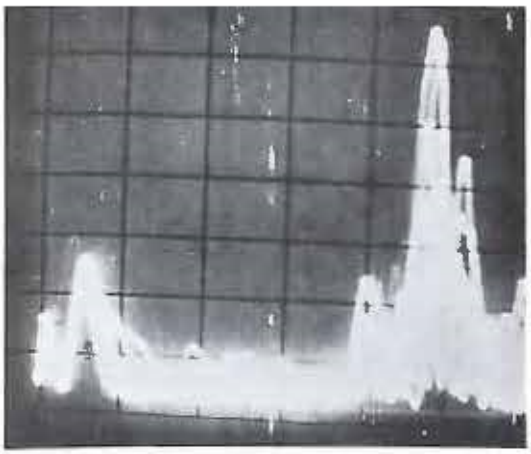

F/A = 0
ATTENUATOR SETTING = 20 db.

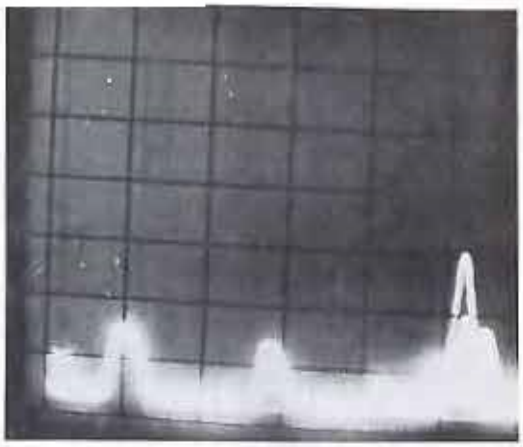

F/A = .012
ATTENUATOR SETTING = 25 db.

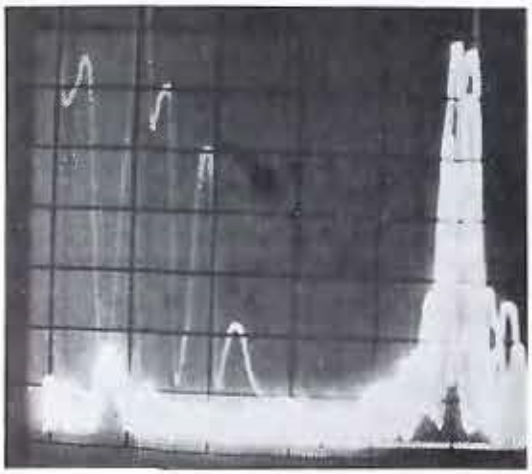

F/A = .004
ATTENUATOR SETTING = 20 db.

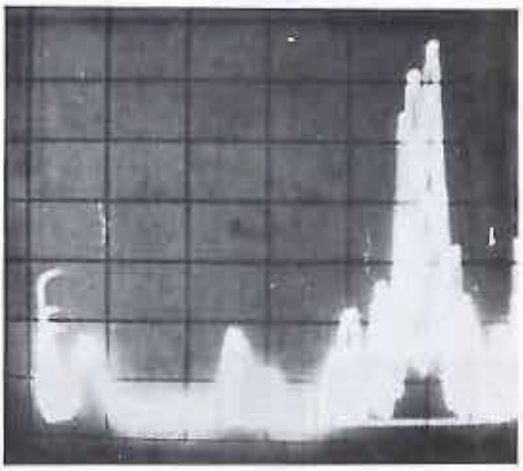

F/A = .016
ATTENUATOR SETTING = 20 db.

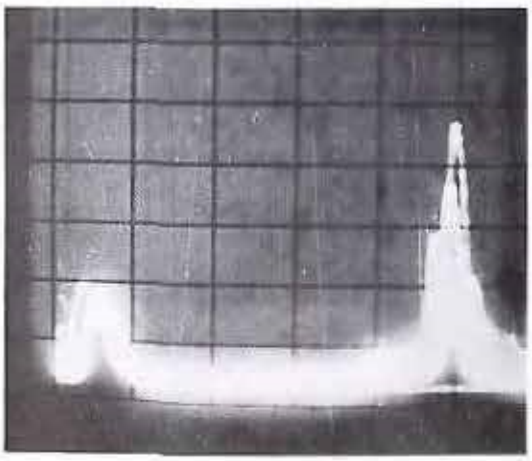

F/A = .008
ATTENUATOR SETTING = 30 db.

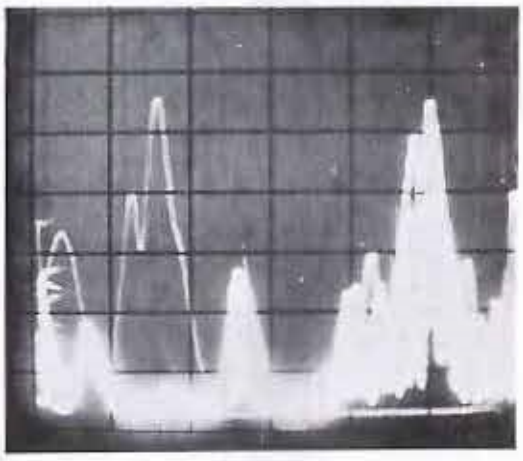

F/A = .020
ATTENUATOR SETTING = 20 db.

PANORAMIC WAVE ANALYSER TRACES FROM ACCELEROMETER ATTACHED TO FLAME TUBE

FREQUENCY RANGE: 0 C.P.S. TO 1000 C.P.S. (APPROX.)
PEAK AT LEFT OF EACH PHOTOGRAPH IS AT 0 C.P.S.

SWEEP TIME = 3 SEC.
EXPOSURE TIME = 30 SEC.

FIG. 23
LR-154

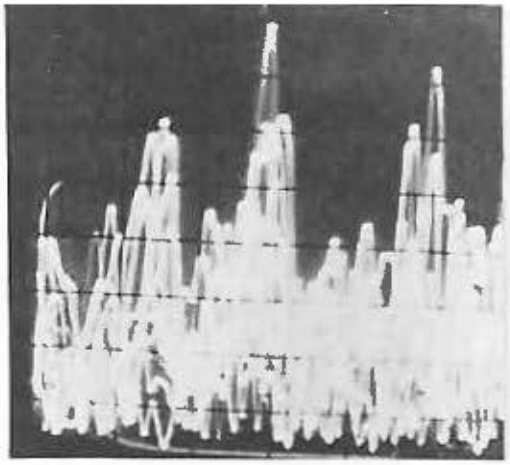

F/A = 0
ATTENUATOR SETTING = 20 db.

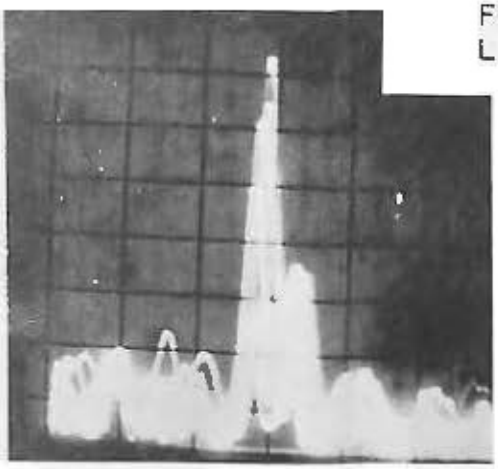

F/A = .012
ATTENUATOR SETTING = 35 db.

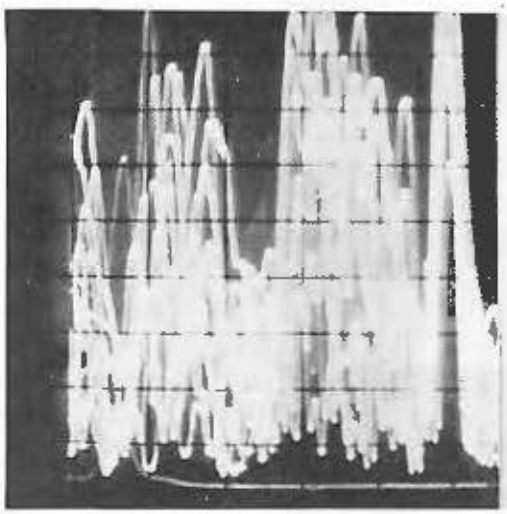

F/A = .004
ATTENUATOR SETTING = 20 db.

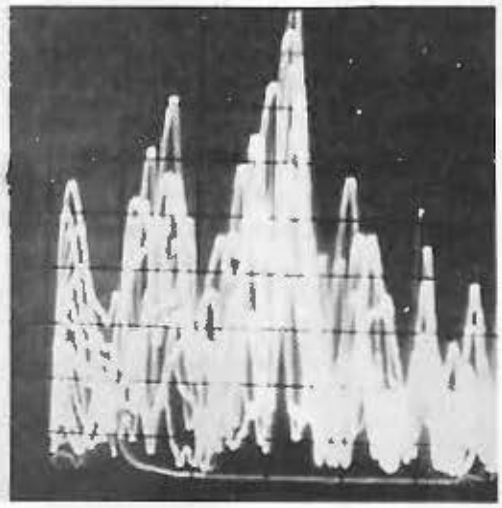

F/A = .016
ATTENUATOR SETTING = 30 db.

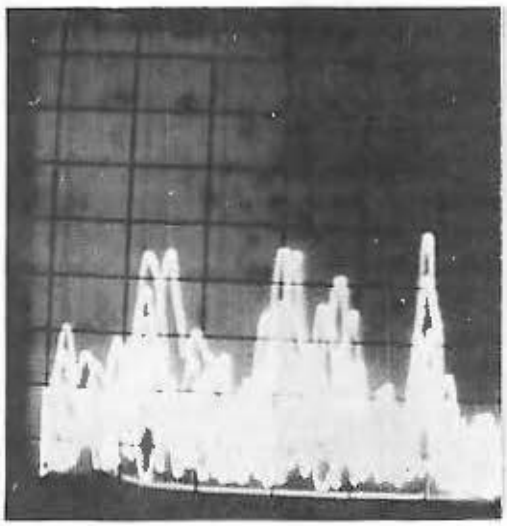

F/A = .008
ATTENUATOR SETTING = 30 db.

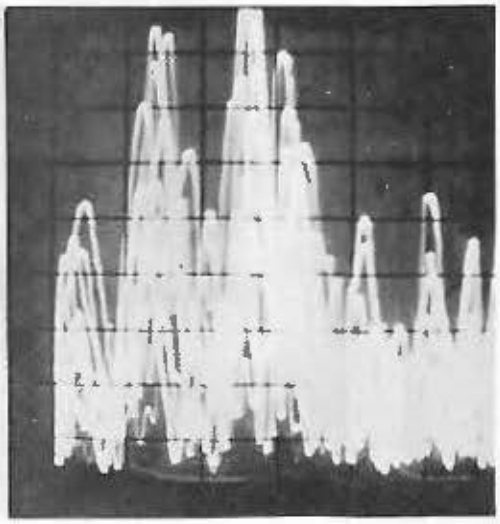

F/A = .020
ATTENUATOR SETTING = 30 db.

PANORAMIC WAVE ANALYSER TRACES FROM MICROPHONE

FREQUENCY RANGE: 0 C.P.S. TO 1000 C.P.S. (APPROX.)
PEAK AT LEFT OF EACH PHOTOGRAPH IS AT 0 C.P.S.

SWEEP TIME = 3 SEC.
EXPOSURE TIME = 30 SEC.

FIG. 24
LR-154

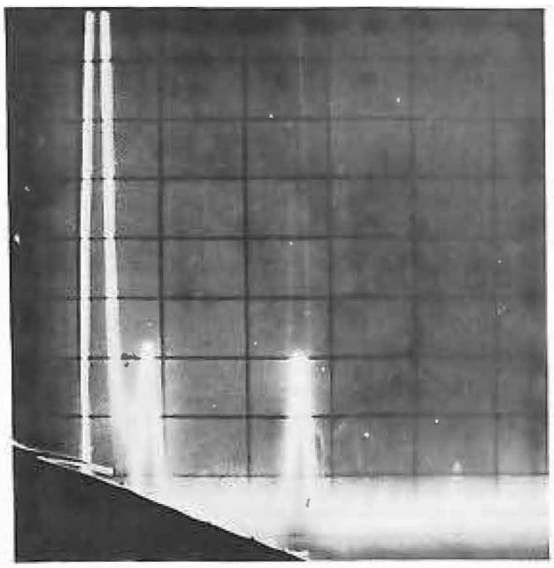

TEST NO. 1

COMBUSTOR BURNING AND PRODUCING HUM. TRANSDUCER CLOSE TO COMBUSTOR. PUMP NO. 1 SUPPLYING FUEL. FUEL PRESSURE PULSATION FREQUENCY = 272 C.P.S.

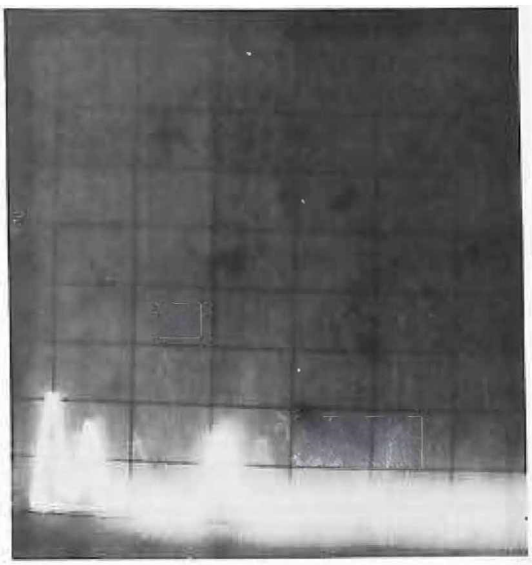

TEST NO. 2

COMBUSTOR NOT BURNING. PUMP NO. 1 RUNNING. TRANSDUCER CLOSE TO PUMP. FUEL PRESSURE PULSATION FREQUENCY = 285 C.P.S.

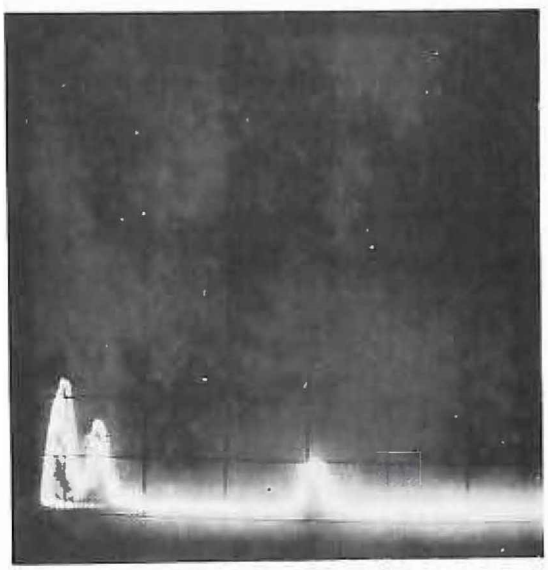

TEST NO. 3

COMBUSTOR NOT BURNING. PUMP NO. 2 RUNNING. TRANSDUCER CLOSE TO PUMP. FUEL PRESSURE PULSATION FREQUENCY = 433 C.P.S.

PANORAMIC WAVE ANALYSER TRACES FROM TRANSDUCER IN FUEL LINE

FREQUENCY RANGE : 0 C.P.S. TO 1000 C.P.S. (APPROX.)

SWEEP TIME = 3 SEC.

EXPOSURE TIME = 30 SEC.

PEAKS AT LEFT OF EACH PHOTOGRAPH ARE AT 0 C.P.S. AND 60 C.P.S. (LINE FREQUENCY)

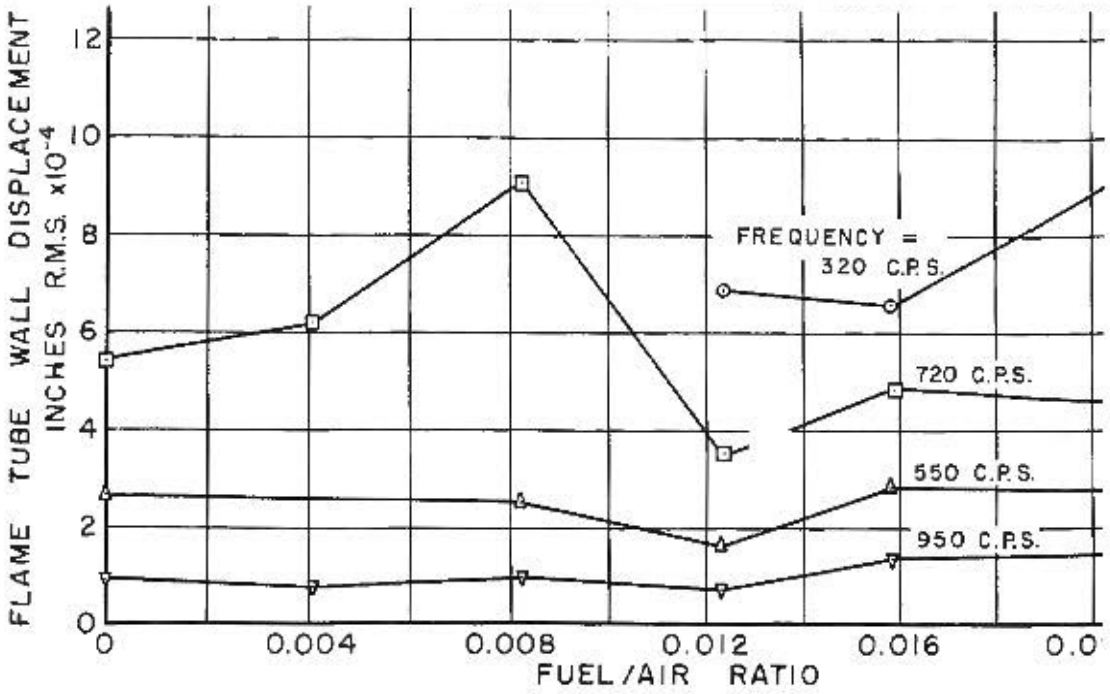

FIG. 25 ANALYSIS OF COMBUSTOR FLAME TUBE W/ TRANSVERSE VIBRATIONS

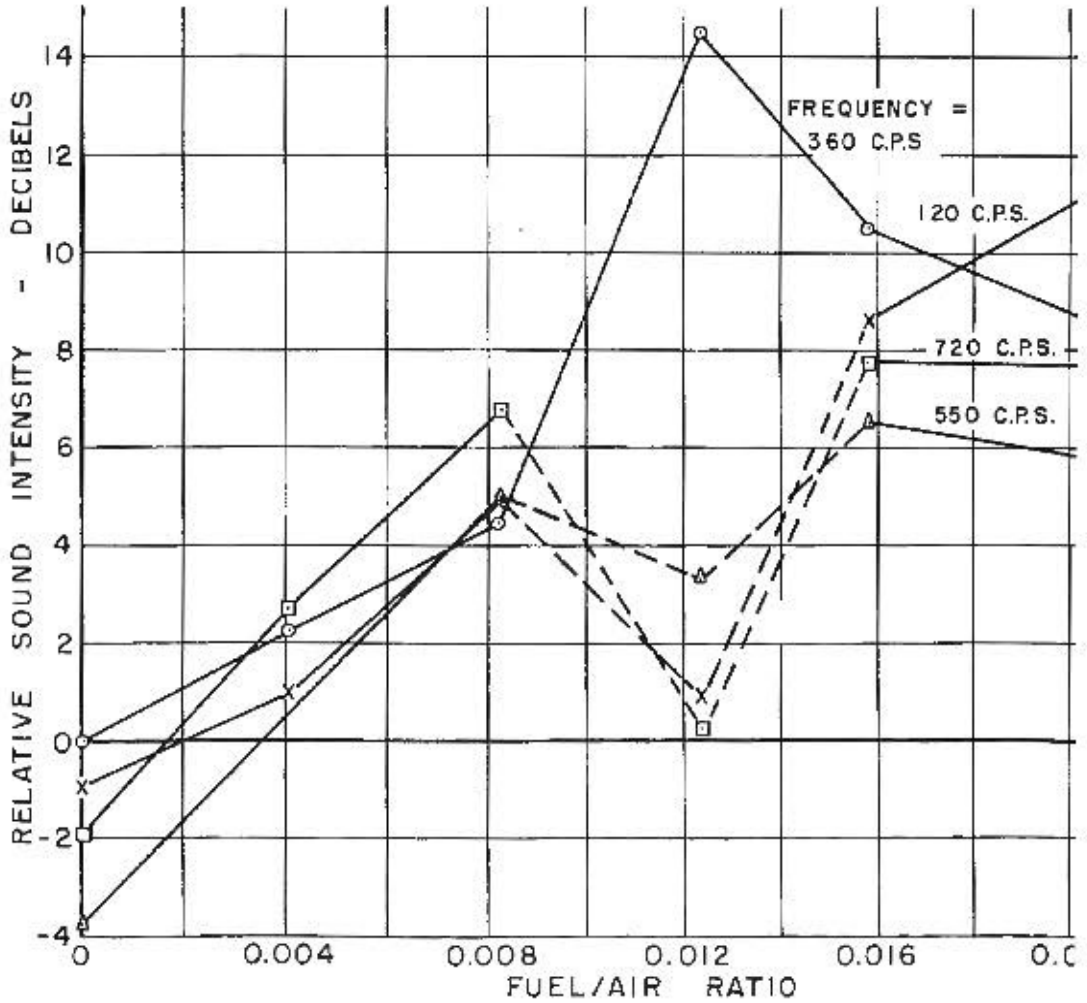

FIG. 26 ANALYSIS OF COMBUSTOR NOISE

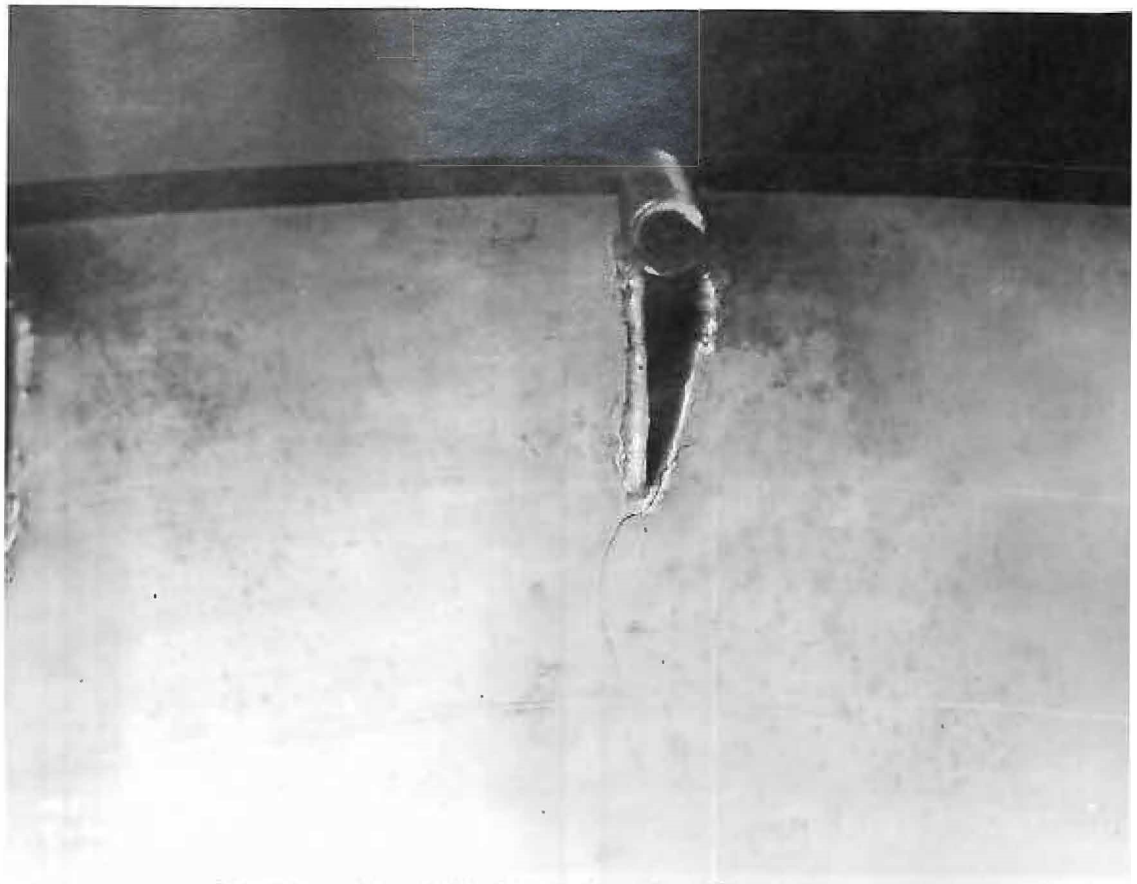

(a) CRACK IN WELD ON INNER WALL OF SNOUT

(b) CRACKS IN WELD ON OUTER WALL OF SNOUT

TOP

BOTTOM

CARBON DEPOSITION ON BASE PLATE, VAPORIZER TUBES,
TOTAL BURNING TIME = 22-23 HR. RICH BURNING TIME = 5

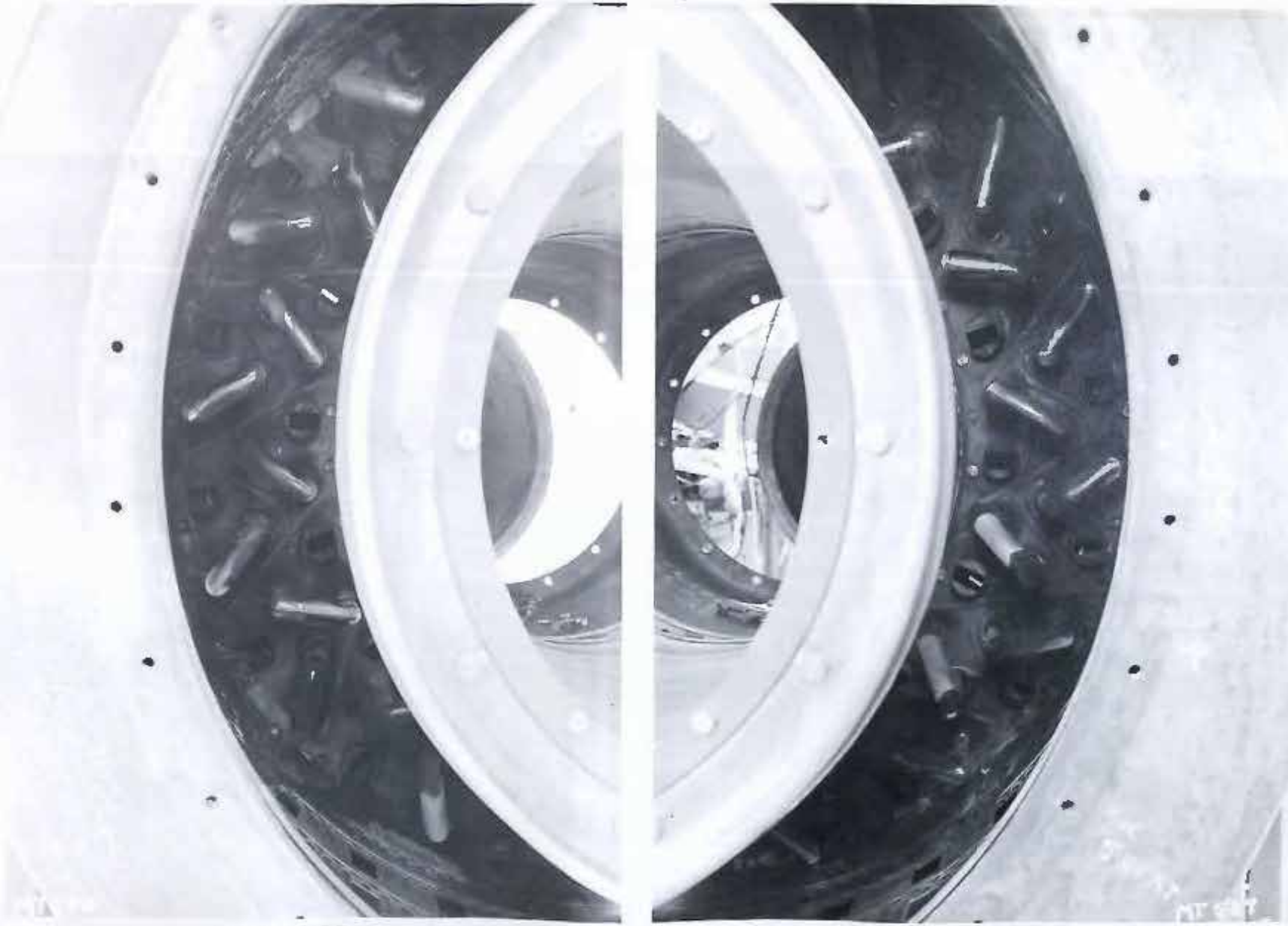

LEFT SIDE RIGHT SIDE

CARBON DEPOSITION ON BASE PLATE, VAPORIZER TUBES, ETC.

TOTAL BURNING TIME = 22-23 HR. RICH BURNING TIME = 5 HR.

FIG. 28 (Cont'd)
LR-154

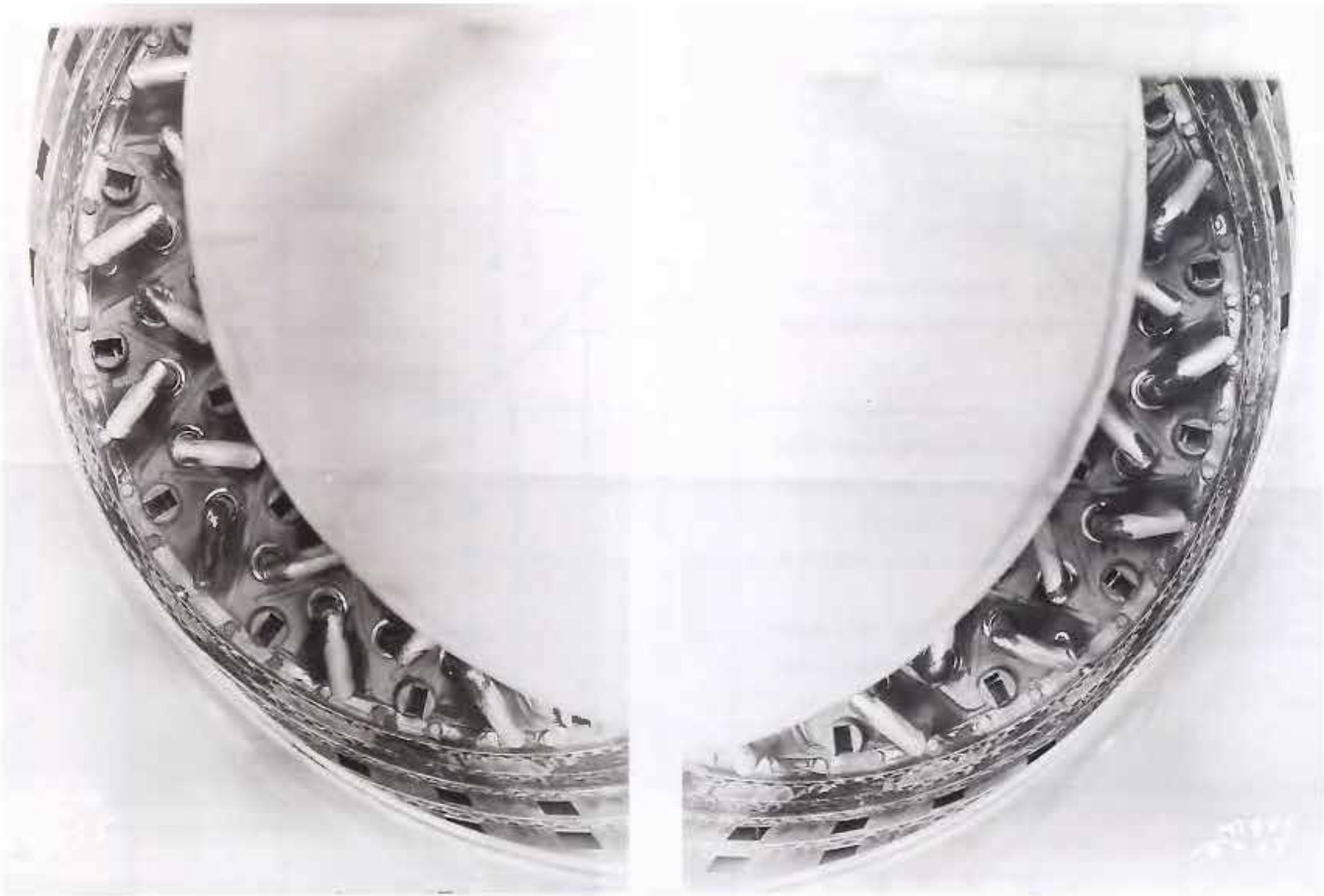

BOTTOM LEFT SIDE

BOTTOM RIGHT SIDE

CARBON DEPOSITION ON BASE PLATE, VAPORIZER TUBES, ETC.

BURNING TIME OF A FEW MINUTES AT LOW FUEL/AIR RATIO FOLLOWING THE CONDITION SHOWN IN FIG. 28

FIG. 29
LR-154

FIG. 30
LR-154

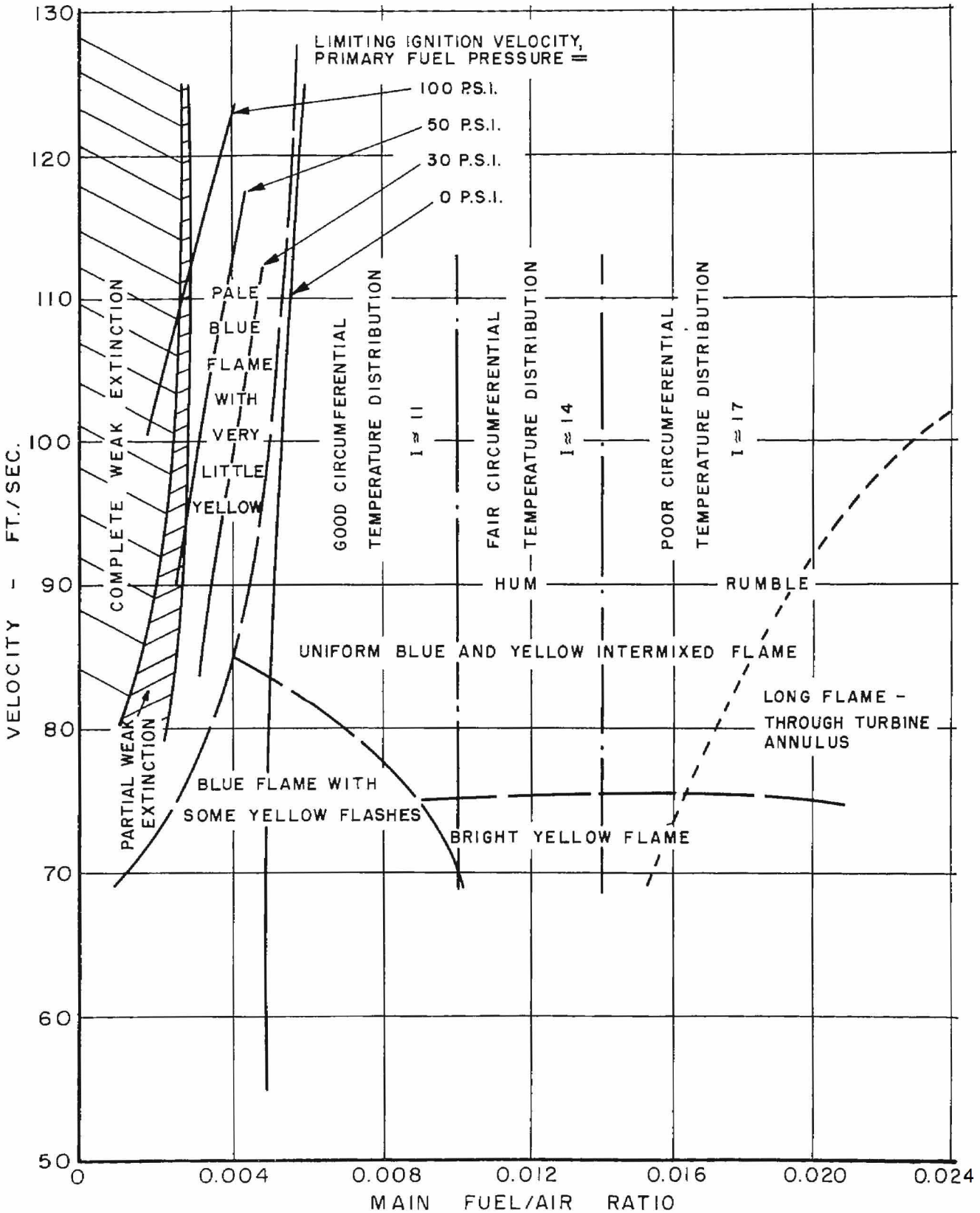

SEMI-QUANTITATIVE SUMMARY OF RESULTS OF TESTS ON STABILITY LIMITS, IGNITION LIMITS, FLAME PATTERNS, OUTLET TEMPERATURE DISTRIBUTIONS, AND COMBUSTION ROUGHNESS

APPENDIX A

CALCULATION OF MEAN TOTAL HEAD PRESSURE IN PLANE D

It was known that the swirl in plane D did not have a constant value of 30 degrees (the angle at which the probes were set) and provisions were made to measure the swirl angle, at least approximately. One of the plane D probes was modified to be rotatable with a scale attached. The pressure reading obtained from each probe hole in turn was maximized by rotating the probe and the corresponding angle read from the scale. This method gave an accurate measure of the maximum total pressure at each hole and a very rough measure of the swirl angle. These measurements were made at the maximum mass flow obtainable only and were only possible in quadrants No. 1, 3, and 4. The results are given in the following table.

	Quadrant No. 1				Quadrant No. 3				Quadrant No. 4			
Hole No.	Pressure in. Hg G.			Angle*	Pressure			Angle*	Pressure			Angle*
	30°	Max.	Diff.		30°	Max.	Diff.		30°	Max.	Diff.	
1	-0.30	- 0.30	0	-	- 0.20	- 0.20	0	-	- 0.50	- 0.50	0	-
2	7.55	7.90	0.35	14°	10.40	10.55	0.15	37°	9.15	9.70	0.55	12
3	9.95	10.60	0.65	36	10.15	10.60	0.45	48	10.50	10.70	0.20	44
4	9.45	10.25	0.80	50	8.00	8.75	0.75	48	9.30	10.10	0.80	48
5	7.30	8.20	0.50	50	7.10	7.50	0.40	44	7.25	7.90	0.65	48
6	6.10	6.35	0.25	47	6.70	7.60	0.90	52	5.80	6.50	0.70	55
Average:			0.51				0.53				0.58	

Average Increase in Pressure = 0.54 in. Hg

* Clockwise from upstream.

It will be noted from Table I and the above table that the reading from hole No. 1 is in all cases approximatel equal to the atmospheric pressure (in some cases slightly below atmospheric) and is uninfluenced by rotating the probe. This indicates that hole No. 1 is in a breakaway region adjacent to the inner wall of the annulus in which the veloci is virtually zero. Hole No. 1 thus indicates the static pres sure in this region which is below the outer wall static pres sure due to the pressure gradient caused by the swirl.

A further limited set of measurements were made in an attempt to determine the total pressure variation between the positions of holes No. 1 and 2. In quadrants No. 1 and 3 the probe, set at 30 degrees, was withdrawn in steps of 1/8 i and the reading taken from hole No. 1. These measurements we made only at the maximum mass flow obtainable. The results a plotted in Figure A-1.

Finally, measurements made by Orenda Engines Limite using a combined yawmeter and total head pressure probe on a similar combustor bearing a close resemblance at plane D to the combustor described in this report revealed that the tota pressure was constant between the inner wall and the position of hole No. 1 and fell linearly between hole No. 6 and the outer wall.

On the basis of these considerations, the following assumptions were made regarding the total head and static pressure profiles of each quadrant in plane D in order to calculate the mean total pressure:

(a) From the inner wall to hole No. 1 the dynamic head is zero and the static pressure at the inner wall equals the reading from hole No. 1

(b) The static pressure varies linearly between the inner and outer walls

(c) The total pressure varies linearly between holes No. 1 and 2

(d) The readings from holes No. 2 to 6 inclusive must be corrected by the addition of an averaged term to allow for maximizing the pressure through setting the correct yaw angle. This correction term has the value of 0.54 in. Hg at a velocit of 120 ft./sec. and is proportional to $(\text{velocity})^2$

(e) The total pressure falls linearly from its correct value at hole No. 6 to the static pressure as read at the outer wall.

The mean total pressure for each quadrant was taken as $\frac{\Sigma MP}{\Sigma M}$ where P = total pressure in any annular subdivision of the full annulus, M = mass flow through the subdivision based on the total and static pressures in that subdivision and the average plane D temperature.

An example of the total and static pressure profiles corrected for swirl, etc. for a typical condition is shown in Figure A-2. The values P_2, P_3, P_4, P_5 and the corresponding static pressures obtained from the curves were used to calculate mass flows in subdivisions A_2, A_3, A_4, A_5. However, no air flows through the innermost half of A_1 and due to the shape of the curve the value P_6 could not be taken as the mean for A_6. Consequently, the mean values of total pressure were obtained from the curves for A_1', A_6' and A_6'' and the mass flows through these annuli calculated separately. The mean total head pressure was then calculated from the expression given above.

This method was used to calculate the mean total pressure at six conditions. It was noticed however that if the readings from holes No. 2 to 6 inclusive on the rakes from Table I were averaged a number was obtained which was very nearly equal to the mean total pressure because the corrections for the swirl and the breakaway in the calculations tended to cancel each other.

A comparison of the results of calculating the mean pressure and averaging the readings from holes No. 2 to 6 is given in the following table.

	Ref. No.	Calculated mean pressure in. Hg Abs.	Average of holes No. 2 to 6 in. Hg Abs.	Error Percent
Screen in place	3	33.02	32.98	0.12
	6	35.88	35.84	0.11
Screen Removed	4	34.18	34.17	0.03
	6	35.52	35.50	0.06
	10	38.29	38.13	0.42
	11	38.84	38.63	0.54

On the basis of these results all the values of mean total head pressure shown in Table II were obtained by the more approximate method which was much simpler and considered to be sufficiently accurate.

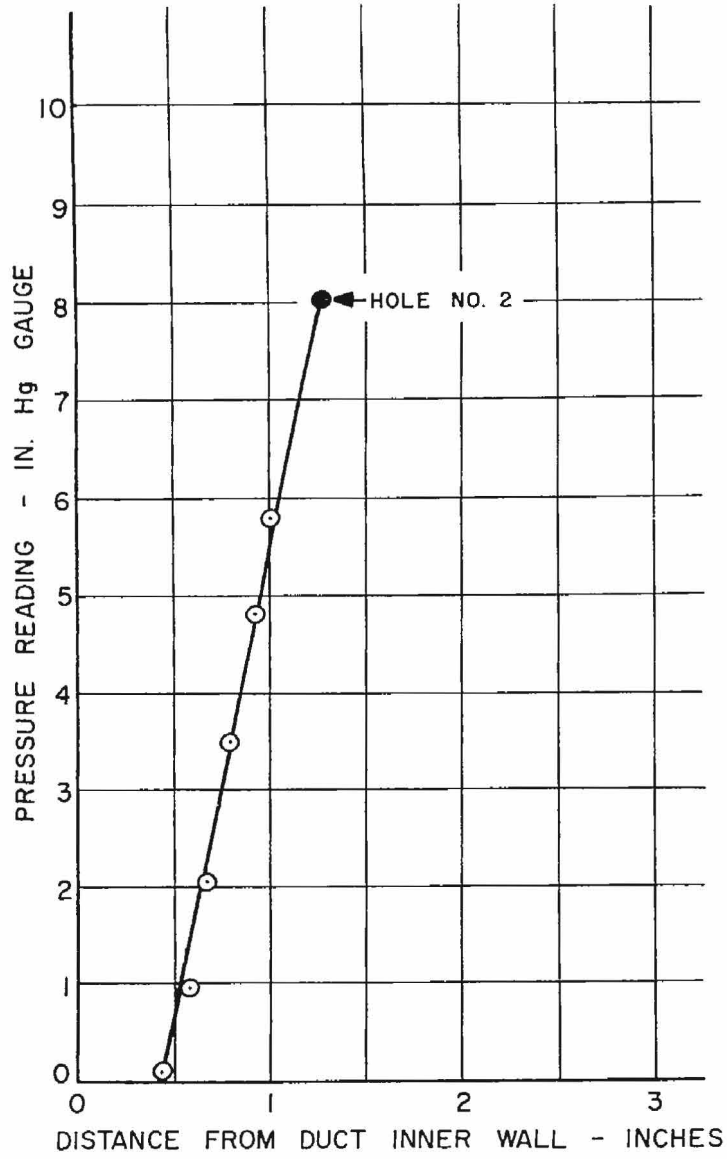

QUADRANT NO. 1, PLANE D

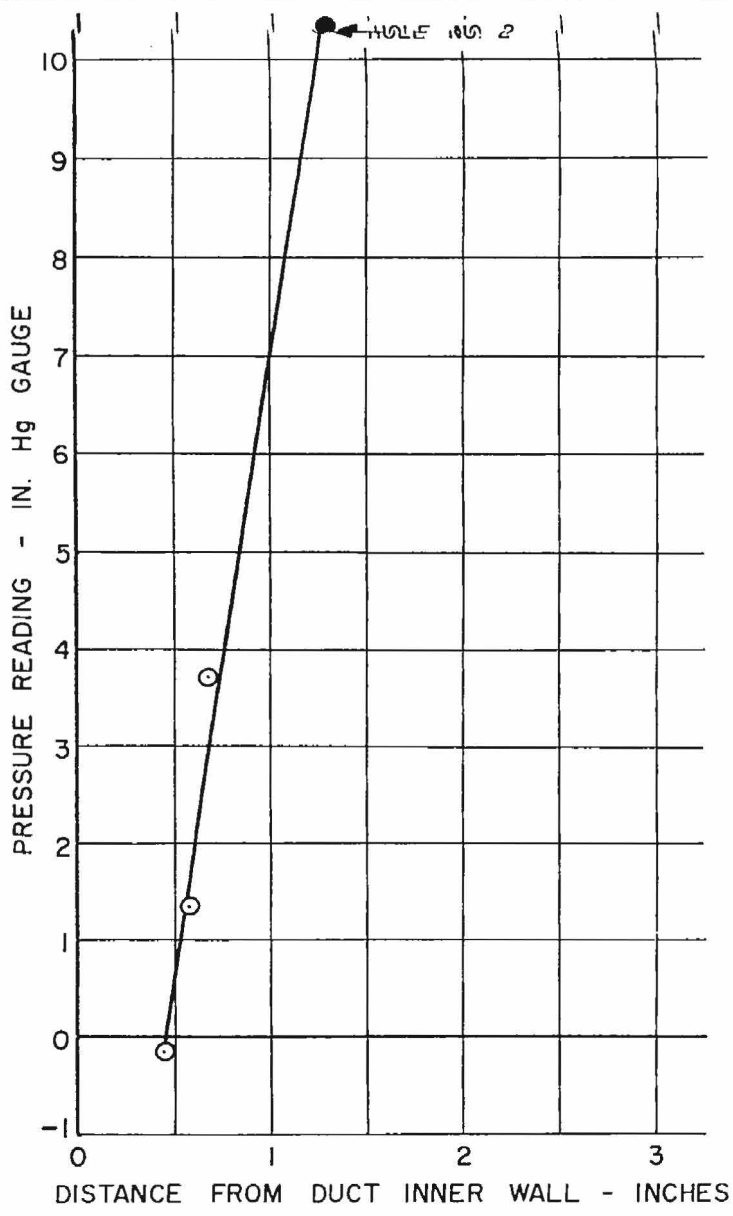

QUADRANT NO. 3, PLANE D

PRESSURE READINGS FROM HOLE NO. 1 OF TOTAL HEAD RAKE WHEN RAKE WITHDRAWN IN STEPS OF 1/8 IN.

FIG. A-1
LR-154

FIG. A-2
LR-154

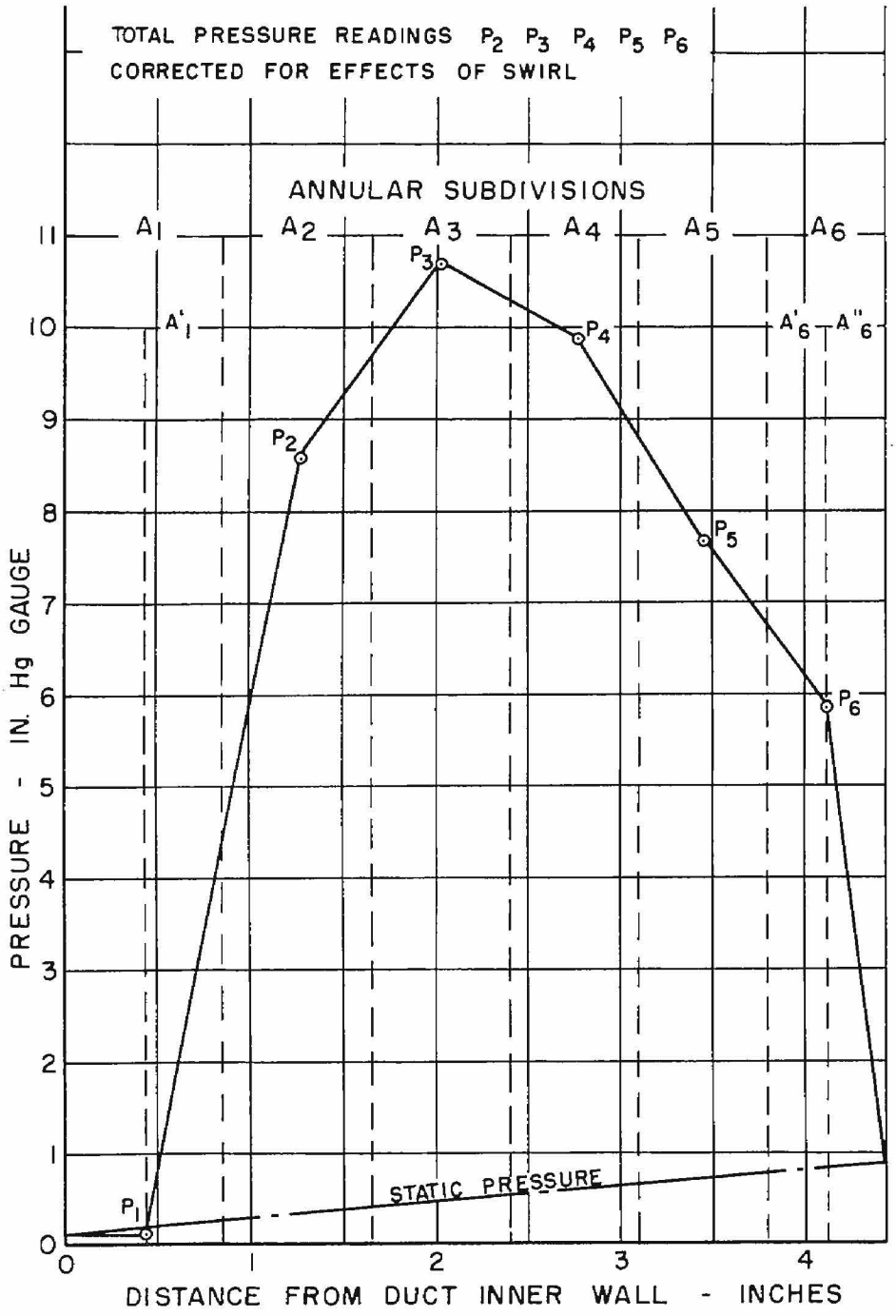

EXAMPLE OF TOTAL AND STATIC PRESSURE PROFILES, PLANE D